Improved light-cone harmonic oscillator model for the ϕ-meson longitudinal leading-twist light-cone distribution amplitude and its effects to $D_s^+ \to \phi \ell^+ \nu_\ell$

Dan-Dan Hu,[1,*] Xing-Gang Wu,[1,†] Long Zeng,[1,‡] Hai-Bing Fu,[2,§] and Tao Zhong[2,‖]

[1]*Department of Physics, Chongqing Key Laboratory for Strongly Coupled Physics, Chongqing University, Chongqing 401331, People's Republic of China*

[2]*Department of Physics, Guizhou Minzu University, Guiyang 550025, People's Republic of China*

(Received 30 April 2024; revised 2 July 2024; accepted 13 August 2024; published 9 September 2024)

In the present paper, we study the properties of ϕ-meson longitudinal leading-twist light-cone distribution amplitude $\phi_{2;\phi}^{\parallel}(x,\mu)$ by starting from a light-cone harmonic oscillator model for its wave function. To fix the input parameters, we derive the first ten order ξ moments of $\phi_{2;\phi}^{\parallel}(x,\mu)$ by using the QCD sum rules approach under the background field theory. The curves of $\phi_{2;\phi}^{\parallel}(x,\mu=2\ \mathrm{GeV})$ tend to be a single-peak behavior, which is consistent with the latest lattice QCD result. To show how the twist-3 light-cone distribution amplitudes (LCDAs) affect the results, we consider two scenarios for the ϕ-meson chiral twist-3 LCDAs $\phi_{3;\phi}^{\perp}(x)$ and $\psi_{3;\phi}^{\perp}(x)$, i.e., the ones using the Wandzura-Wilczek approximation with $\phi_{2;\phi}^{\parallel}(x,\mu)$ (S1) and the ones using self-consistent conformal expansion with second-order Gegenbauer moments $a_{2;\phi}^2$ in this work (S2). As an application, we derive the $D_s^+ \to \phi$ transition form factors (TFFs) by using the QCD light-cone sum rules. The TFFs at large recoil point for those two scenarios are given separately. As for the two TFF ratios γ_V and γ_2, we obtain $\gamma_V^{(\mathrm{S1})} = 1.755^{+0.008}_{-0.005}$, $\gamma_2^{(\mathrm{S1})} = 0.852^{+0.135}_{-0.133}$, $\gamma_V^{(\mathrm{S2})} = 1.723^{+0.023}_{-0.021}$, and $\gamma_2^{(\mathrm{S2})} = 0.785^{+0.100}_{-0.104}$. After extrapolating those TFFs to the physically allowable region, we then obtain the transverse, longitudinal, and total decay widths for semileptonic decay $D_s^+ \to \phi \ell^+ \nu_\ell$. Then the branching fractions are $\mathcal{B}^{(\mathrm{S1})}(D_s^+ \to \phi e^+ \nu_e) = (2.347^{+0.342}_{-0.191}) \times 10^{-3}$, $\mathcal{B}^{(\mathrm{S1})}(D_s^+ \to \phi \mu^+ \nu_\mu) = (2.330^{+0.341}_{-0.190}) \times 10^{-3}$, $\mathcal{B}^{(\mathrm{S2})}(D_s^+ \to \phi e^+ \nu_e) = (2.367^{+0.256}_{-0.132}) \times 10^{-3}$, and $\mathcal{B}^{(\mathrm{S2})}(D_s^+ \to \phi \mu^+ \nu_\mu) = (2.349^{+0.255}_{-0.132}) \times 10^{-3}$, which show good agreement with the data issued by the BESIII, CLEO, and *BABAR* Collaborations. We finally calculate $D_s^+ \to \phi \ell^+ \nu_\ell$ polarization and asymmetry parameters, which can be measured and tested in future experiments.

DOI: 10.1103/PhysRevD.110.056017

I. INTRODUCTION

The heavy-to-light semileptonic decay is an ideal platform for exploring the properties of the involved heavy quark and the light meson and for testing the standard model (SM). It also presents a remarkable opportunity to scrutinize lepton flavor universality (LFU) and to explore the potential manifestations of new physics beyond the SM. For the D_s^+-meson semileptonic decay, $D_s^+ \to \phi \ell^+ \nu_\ell$, it is important because the ϕ meson with $J^{\mathrm{PC}} = 1^{--}$ is constructed by the $(s\bar{s})$ component within the valance quark model with a narrow resonance that can be well isolated experimentally. Therefore, accurately determining the branching fraction for $D_s^+ \to \phi \ell^+ \nu_\ell$ is crucial for studying the properties of ϕ and provides a complementary examination for LFU.

In the early 1990s, the Fermilab E687, E791, CLEO, and FOCUS Collaborations explored this channel through photoproduction processes [1–5]. During the past two decades, the *BABAR* Collaboration presented the branching fraction $\mathcal{B}(D_s^+ \to \phi \ell^+ \nu_\ell) = (2.61 \pm 0.03 \pm 0.17)\%$ in a relative measurement using a 10 MeV mass requirement for $\phi \to K^+K^-$ and taking $D_s^+ \to K^+K^-\pi^+$ as their reference mode [6]. In 2015, CLEO Collaboration used their measured $D_s^+ \to f_0 e^+ \nu_e$ branching fraction and Flatté

*Contact author: hudd@stu.cqu.edu.cn
†Contact author: wuxg@cqu.edu.cn
‡Contact author: zlong@cqu.edu.cn
§Contact author: fuhb@cqu.edu.cn
‖Contact author: zhongtao1219@sina.com

model-based Monte Carlo simulations to obtain electron channel branching fraction of $D_s^+ \to \phi e^+ \nu_e$ [7]. In 2017, the BESIII Collaboration reported the $D_s^+ \to \phi \ell^+ \nu_\ell$ branching fraction for muon channels [8]. However, there is a little gap in the branching fractions between the electron and muon channels. Recently in 2023, BESIII updated the absolute branching fraction for $D_s^+ \to \phi \mu^+ \nu_\mu$ [9]. Those data give us good chances for exploring and testing the nonperturbative properties of D_s^+ and ϕ mesons.

The $D_s^+ \to \phi$ transition is the key component for studying the decay channel $D_s^+ \to \phi \ell^+ \nu_\ell$, which can be decomposed into four transition form factors (TFFs) due to the Lorentz structure of its hadronic matrix element [10]. These TFFs, which incorporate nonperturbative effects due to the large QCD coupling constant in the low q^2 region and the bound state effects in the large q^2 region, have been treated under various approaches. Specifically, the $D_s^+ \to \phi$ TFFs have been calculated by using the traditional three-point sum rules (3PSRs) [10,11], the light-cone sum rules (LCSRs) in the framework of heavy quark effective field theory (HQEFT) [12,13], the heavy meson chiral Lagrangians (HMχT) [14], the covariant quark model (CQM) [15,16], the covariant confining quark model (CCQM) [17], the covariant light-front quark model (CLFQM) [18–20], the light-front quark model (LFQM) [21], the lattice QCD (LQCD) [22–24], the chiral unitary approach (χUA) [25,26], the relativistic quark model (RQM) [27], and the symmetry-preserving regularization of a vector × vector contact interaction (SCI) [28]. Those approaches are valid in different q^2 regions. For example, the QCD sum rules (QCD SRs) approach, either the LCSR or the 3PSR, is applicable for the relatively low and intermediate q^2 regions, while the LQCD and the HMχT are applicable for the large q^2 region. Predictions of heavy-to-light TFFs under various approaches are complementary to each other [29]. Moreover, it has been pointed out that it is better to adopt the LCSR approach, instead of the QCD sum rules approach [30,31], to deal with the heavy-to-light TFFs [32–35]. The QCD sum rules deals with the nonperturbative hadron phenomenology by expanding the correlation function into the QCD vacuum condensates. Comparing with the QCD sum rules, a two-point correlation function (correlator) is introduced in the LCSR approach for the heavy-to-light TFFs, which can be expanded near the light cone $x^2 \to 0$, whose matrix elements are then parameterized as the light meson's light-cone distribution amplitudes (LCDAs) of increasing twists. Because the LCSR prediction is applicable in a wider region and can be adapted for all q^2 regions via proper extrapolations, in this paper, we will adopt the LCSR approach to calculate TFFs. It is noted that the previous LCSR predictions of the $D_s^+ \to \phi$ TFFs and their related ratios r_2 and r_V [13] exhibit significant discrepancies with the experimental measurements. Therefore, it is crucial to recalculate them.

In the LCSR, the notion of the LCDAs refers to matrix elements of nonlocal operators sandwiched between the hadron state and the vacuum. The LCDAs have direct physical significance and provide the underlying links between the hadronic phenomena at small and large distances. It is worth noting that the heavy-to-light TFFs at the large recoil point can be typically affected by $\mathcal{O}(10\%)$ by the nonasymptotic terms of LCDAs in the LCSR approach, cf. Refs. [36–40]. Thus, the s-quark mass effect need to be taken into consideration for a careful study on the properties of ϕ mesons. Normally, the twist-2 (or, equivalently, called the leading-twist) LCDA gives dominant contribution in the pseudoscalar meson. The cases are different in the vector meson in which the twist-3 LCDA also has large contributions in the TFFs. So the longitudinal leading-twist and chiral-odd twist-3 ϕ-meson LCDAs are the focus in this paper. At present, the ϕ-meson leading-twist LCDA has been calculated by using the QCD SR [41,42], Dyson-Schwinger equation (DSE) [43], Bethe-Salpeter wave functions (BSWFs) [44], and the algebraic model (AM) [45], etc. In 2022, the LCDAs of the longitudinally and transversely polarized ϕ meson have been calculated by using the lattice QCD based on the large momentum effective theory [46]. At present, various theoretical predictions for the ϕ meson's leading-twist LCDAs still exhibit a discrepancy, which also motivates this work.

Generally, the LCDA can be obtained by integrating over the transverse momentum dependence of the light-cone wave function (LCWF). In this paper, we will first construct a light-cone harmonic oscillator (LCHO) model for the ϕ-meson leading-twist LCWF based on the Brodsky-Huang-Lepage (BHL) prescription [47–49], which will then be applied to constrain the behavior of ϕ-meson longitudinal leading-twist LCDA $\phi_{2;\phi}^{\parallel}(x,\mu)$. The BHL prescription constructs the light meson's LCWF by connecting the equal-time wave function in the rest frame and the wave function in the infinite momentum frame. We will take two ways (called model I and model II, respectively) to fix the input parameters of $\phi_{2;\phi}^{\parallel}(x,\mu)$, both of which need to know the moments of $\phi_{2;\phi}^{\parallel}(x,\mu)$. For this purpose, we will calculate the wanted moments by using the QCD SR within the framework of background field theory (BFTSR). The key idea of the background field theory is to describe the nonperturbative effects with the classical background field satisfying the equation of motion and to describe the quantum fluctuation on this basis within the framework of quantum field theory [50–52]. The BFTSR method provides a systematic description of the vacuum condensates from the field theory point of view and a viable way to consider the nonperturbative effects. By taking the QCD background field as the starting point for the QCD sum

rules, it not only shows a distinct physical picture but also greatly simplifies the calculation due to its capability of adopting different gauge conditions for the quantum fluctuations and backgrounds, respectively. More explicitly, the vacuum expectation values of the background fields well describe the nonperturbative effects, while the quantum fluctuations represent the calculable perturbative effects.

The LCDA can reflect the dynamic information of the hadron internal structure and is the basic parameter of the hard exclusive process. Normally, the ϕ-meson longitudinal leading-twist LCDA at scale μ is written as a Gegenbauer polynomial series, e.g.,

$$\phi^{\parallel}_{2;\phi}(x,\mu) = 6x(1-x)\left[1+\sum_{n=2}^{n} a^{n}_{2;\phi}(\mu) C_n^{3/2}(2x-1)\right], \quad (1)$$

where $C_n^{3/2}(2x-1)$ is the nth-order Gegenbauer polynomial, and $a^n_{2;\phi}(\mu)$ is the corresponding Gegenbauer moment. Because of the conservation of G parity, all the odd Gegenbauer moments vanish, and only the even Gegenbauer moments are retained. Normally the LCDA model based on conformal expansion is truncated after the first few terms, which, however, is not suitable for all cases, since the higher-order Gegenbauer moments may also have considerable contributions. Therefore, understanding more moments is important for accurately determining the LCDA. However, with the increasing of n, the stability of the Gegenbauer moment will decline sharply, and the obtained LCDA will no longer converge, resulting in inaccurate predictions. Thus, it is helpful to have an improved ϕ-meson longitudinal twist-2 LCDA model, as is the purpose of the present paper.

Model I is followed from the usual idea that the LCDA can be expanded as a Gegenbauer polynomial series, the nth-order Gegenbauer moment $a^n_{2;\phi}(\mu)$ will first be determined by using the moments of $\phi^{\parallel}_{2;\phi}(x,\mu)$, and then the parameters of $\phi^{\parallel}_{2;\phi}(x,\mu)$ will be fixed by using the following equation:

$$a^n_{2;\phi}(\mu) = \frac{\int_0^1 \mathrm{d}x \phi^{\parallel}_{2;\phi}(x,\mu) C_n^{3/2}(2x-1)}{\int_0^1 \mathrm{d}x 6x(1-x)[C_n^{3/2}(2x-1)]^2}. \quad (2)$$

As for model II, the least squares method will be first employed to fix the nth-order moment $\langle \xi^{\parallel;n}_{2;\phi}\rangle$, which will be directly adopted for determining the input parameters of $\phi^{\parallel}_{2;\phi}(x,\mu)$ by using the definition

$$\langle \xi^{\parallel;n}_{2;\phi}\rangle|_{\mu} = \int_0^1 \mathrm{d}x (2x-1)^n \phi^{\parallel}_{2;\phi}(x,\mu), \quad (3)$$

where μ represents some initial scale.

Furthermore, the ϕ-meson chiral-odd twist-3 LCDAs $\phi^{\perp}_{3;\phi}(x)$ and $\psi^{\perp}_{3;\phi}(x)$ also have significant contributions to the charmed meson semileptonic decays, since they have large contributions to the related TFFs. Early in 1998, they were researched by using the simplest but self-consistent conformal expansion, which satisfies the QCD equations of motion suggested by Ball and Braun [53]. Meanwhile, the $\phi^{\perp}_{3;\phi}(x)$ and $\psi^{\perp}_{3;\phi}(x)$ can be decomposed into several terms, the twist-2 distribution amplitudes (Wandzura-Wilczek part), the three-particle distribution amplitudes, and the quark-mass correction terms. Normally, the three-particle distribution amplitudes and the quark-mass correction terms have smaller contributions. Under the Wandzura-Wilczek (WW) approximation, they have the following forms [54,55][1]:

$$\phi^{\perp(\mathrm{WW})}_{3;\phi}(x) = \frac{1}{2}\left[\int_0^x \mathrm{d}v \frac{\phi^{\parallel}_{2;\phi}(v)}{\bar{v}} + \int_x^1 \mathrm{d}v \frac{\phi^{\parallel}_{2;\phi}(v)}{v}\right],$$
$$\psi^{\perp(\mathrm{WW})}_{3;\phi}(x) = 2\left[\bar{x}\int_0^x \mathrm{d}v \frac{\phi^{\parallel}_{2;\phi}(v)}{\bar{v}} + x\int_x^1 \mathrm{d}v \frac{\phi^{\parallel}_{2;\phi}(v)}{v}\right]. \quad (4)$$

Here $\bar{v} = (1-v)$ and $\bar{x} = (1-x)$. In this paper, we will take those two forms into consideration.

The remaining parts of the paper are organized as follows. In Sec. II, we describe the calculation technology for deriving the moments of the ϕ-meson longitudinal leading-twist LCDA $\phi^{\parallel}_{2;\phi}(x,\mu)$ and for the construction of the LCHO model and the determination of its input parameters. Then we given the formulas for the $D_s^+ \to \phi$ TFFs and the transverse, longitudinal, and total decay widths for the semileptonic decay $D_s^+ \to \phi \ell^+ \nu_\ell$. In Sec. III, we present the detailed numerical analysis and discussion. Section IV is reserved for a brief summary.

II. CALCULATION TECHNOLOGY

A. The ξ moments of ϕ-meson longitudinal leading-twist LCDA

The calculation of the form factors for the heavy-to-light transition is primarily influenced by the leading-twist LCDAs of the final state light mesons. To ensure a reasonable distribution amplitude, it is necessary to compute the moments of the corresponding distribution amplitude. The two-particle distribution amplitudes are defined as matrix elements of quark-antiquark gauge-invariant nonlocal operators at lightlike separations. The quark composition of the ϕ meson is $s\bar{s}$, and its corresponding longitudinal leading-twist LCDA $\phi^{\parallel}_{2;\phi}(x,\mu)$ can be defined as [37,38]

$$\langle 0|\bar{s}(z)\gamma_\mu s(-z)|\phi(q,\lambda)\rangle = m_\phi f^{\parallel}_{\phi}\int_0^1 \mathrm{d}x e^{i(xz\cdot q - \bar{x}z\cdot q)} q_\mu \times \frac{e^{*(\lambda)}\cdot z}{q\cdot z}\phi^{\parallel}_{2;\phi}(x,\mu). \quad (5)$$

[1]The WW approximation can be found in Eqs. (4.15) and (4.16) of Ref. [53].

The $f_\phi^\parallel$ is the ϕ-meson longitudinal decay constant. In the above definitions, q and $e^{*(\lambda)}$ are the momentum and polarization vector of the ϕ meson, respectively. The integration variable x corresponds to the momentum fraction carried by the quark. The polarization vector satisfies the relationship $(e^{*(\lambda)}\cdot z)/(q\cdot z)\to 1/m_\phi$ [37]. Performing a series expansion on both sides of Eq. (5) at the lightlike separation z_μ with $z=0$, we obtain

$$\langle 0|\bar{s}(0)\not{z}(iz\cdot\overleftrightarrow{D})^n s(0)|\phi(q,\lambda)\rangle = (z\cdot q)^{n+1} f_\phi^\parallel \langle \xi_{2;\phi}^{n;\parallel}\rangle|_\mu, \quad (6)$$

where the covariant derivative satisfies the relation $(iz\cdot\overleftrightarrow{D})^n = (iz\cdot\vec{D} - iz\cdot\overleftarrow{D})^n$.

In order to determine the sum rules for the moments of ϕ-meson longitudinal distribution amplitude, we adopt the following correlator:

$$\Pi_{2;\phi}^{(n,0)}(z,q) = i\int \mathrm{d}^4x e^{iq\cdot x}\langle 0|T\{J_n(x), J_0^\dagger(0)\}|0\rangle = (z\cdot q)^{n+2} I_{2;\phi}^{(n,0)}(q^2), \quad (7)$$

where $J_n(x)=\bar{s}(x)\not{z}(iz\cdot\overleftrightarrow{D})^n s(x)$ and $J_0^\dagger(0)=\bar{s}(0)\not{z}s(0)$ are interpolating currents. Because of the conservation of G parity, only even moments of $\phi_{2;\phi}^\parallel(x,\mu)$ are nonzero, i.e., $n=(0,2,4,6,\ldots)$. By combining Feynman rules within the framework of BFTSR, one can apply the operator product expansion (OPE) for the correlator (7) in the deep Euclidean region $q^2\ll 0$. Then, the correlator can be expanded into three terms, including the quark propagators $S_F^s(0,x)$, $S_F^s(x,0)$ and the vertex operators $(iz\cdot\overleftrightarrow{D})^n$, which have been given in our previous work [56]. The $S_F^s(0,x)$ and $S_F^s(x,0)$ represent s-quark propagators from 0 to x and x to 0, respectively. When dealing with the Lorentz-invariant scalar function $\Pi_{2;\phi}^{(n,0)}(z,q)$, the OPE yields a series of local operators of increasing dimension. The expectation values of these operators in the nonperturbative (physical) vacuum are known as vacuum condensates, whose detailed expression can be found in Refs. [56,57]. On the other hand, one can insert a complete set of hadronic states intermediated by the ϕ meson with the same J^P quantum number into the correlator and consequently obtain

$$\mathrm{Im}I_{2;\phi,\mathrm{Had}}^{(n,0)}(q^2) = \pi\delta(q^2-m_\phi^2)(f_\phi^\parallel)^2\langle\xi_{2;\phi}^{\parallel;n}\rangle|_\mu\langle\xi_{2;\phi}^{\parallel;0}\rangle + \mathrm{Im}I_{2;\phi}^{\mathrm{pert}}(s)\theta(s-s_\phi), \quad (8)$$

where s_ϕ is the continuum threshold. Finally, the explicit expression for the moments of the distribution amplitudes can be obtained by equating the OPE results with the hadronic representation using the dispersion relation and then performing a Borel transformation. The sum rules for the moment of the ϕ-meson leading-twist LCDA is given by

$$\begin{aligned}
\frac{(f_\phi^\parallel)^2\langle\xi_{2;\phi}^{\parallel;n}\rangle|_\mu\langle\xi_{2;\phi}^{\parallel;0}\rangle|_\mu}{M^2e^{m_\phi^2/M^2}} &= \frac{1}{\pi}\frac{1}{M^2}\int_{4m_s^2}^{s_\phi}\mathrm{d}s e^{-s/M^2}\mathrm{Im}I_{2;\phi}^{\mathrm{pert}}(s) + \frac{2m_s\langle\bar{s}s\rangle}{M^4} + \frac{\langle\alpha_sG^2\rangle}{12\pi M^4}\frac{1+n\theta(n-2)}{n+1} - \frac{8n+1}{9}\frac{m_s\langle g_s\bar{s}\sigma TGs\rangle}{M^6} \\
&+ \frac{\langle g_s\bar{s}s\rangle}{81M^6}4(2n+1) - \frac{\langle g_s^3fG^3\rangle}{48\pi^2M^6}n\theta(n-2) + \frac{\sum\langle g_s^2\bar{q}q\rangle^2}{486\pi^2M^6}\left\{-2(51n+25)\left(-\ln\frac{M^2}{\mu^2}\right)\right. \\
&\left. + 3(17n+35) + \theta(n-2)\left[2n\left(-\ln\frac{M^2}{\mu^2}\right) - 25(2n+1)\tilde{\psi}(n) + \frac{1}{n}(49n^2+100n+56)\right]\right\} \\
&+ m_s^2\left\{-\frac{\langle\alpha_sG^2\rangle}{6\pi M^6}\left[\theta(n-2)(n\tilde{\psi}(n)-2) - n - 2 + 2n\left(-\ln\frac{M^2}{\mu^2}\right)\right]\right. \\
&+ \frac{\langle g_s^3fG^3\rangle}{288\pi^2M^8}\left\{-10\delta^{n0} + \theta(n-2)\left[4n(2n-1)\left(-\ln\frac{M^2}{\mu^2}\right) - 4n\tilde{\psi}(n) + 8(n^2-n+1)\right]\right. \\
&\left. + \theta(n-4)[2n(8n-1)\tilde{\psi}(n) - (19n^2+19n+6)] + 8n(3n-1)\left(-\ln\frac{M^2}{\mu^2}\right) - (21n^2+53n-6)\right\} \\
&- \frac{\sum\langle g_s^2q\bar{q}\rangle^2}{972\pi^2M^8}\left\{6\delta^{n0}\left[16\left(-\ln\frac{M^2}{\mu^2}\right) - 3\right] + \theta(n-2)\left[8(n^2+12n-12)\left(-\ln\frac{M^2}{\mu^2}\right)\right.\right. \\
&\left. - 2(29n+22)\tilde{\psi}(n) + 4\left(5n^2-2n-33+\frac{46}{n}\right)\right] + \theta(n-4)[2(56n^2-25n+24)\tilde{\psi}(n) \\
&\left.\times(139n^2+91n+54)] + 8(27n^2-15n-11)\left(-\ln\frac{M^2}{\mu^2}\right) - 3(63n^2+159n-50)\right\} \\
&\left. + \frac{4(n-1)}{3}\frac{m_s\langle\bar{s}s\rangle}{M^6} + \frac{8n-3}{9}\frac{m_s\langle g_s\bar{s}\sigma TGs\rangle}{M^8} - \frac{4(2n+1)}{81}\frac{\langle g_s\bar{s}s\rangle^2}{M^8}\right\}, \quad (9)
\end{aligned}$$

where M is the Borel parameter, which is an important parameter for determining the LCDA. The QCD SR can be derived accordingly, and its related vacuum condensates are arranged by their mass dimensions. For example, the vacuum condensates $\langle\bar{s}s\rangle$, $\langle\alpha_s G^2\rangle$, $\langle g_s\bar{s}\sigma TGs\rangle$, and $\langle g_s^3 fG^3\rangle$ represent the dimension-three s quark and $\bar{s}$-quark condensate, the dimension-four double-gluon condensate, the dimension-five quark-gluon mixed condensate, and the dimension-six triple-gluon condensate, respectively. $\langle g_s\bar{s}s\rangle^2$ and $\langle g_s^2\bar{q}q\rangle^2$ are two types of dimension-six four-quark condensates. The imaginary part of the perturbative contribution is

$$\mathrm{Im}I^{\mathrm{pert}}_{2;\phi}(s)=\frac{3v^{n+1}}{8\pi(n+1)(n+3)}\left\{[1+(-1)^n](n+1)\times\frac{1-v^2}{2}+[1+(-1)^n]\right\},\tag{10}$$

where $v^2=1\text{–}4m_s^2/s$ and $\tilde{\psi}(n)=\psi(\frac{n+1}{2})-\psi(\frac{n}{2})+\ln 4$. The zeroth-order derivative of the digamma function is given by $\psi(n+1)=\sum_{k=1}^{n}1/k-\gamma_E$ with the Euler constant $\gamma_E=0.577216$. Equation (9) indicates that the zeroth-order ξ moment $\langle\xi^{\|;0}_{2;\phi}\rangle|_\mu$ cannot be normalized in the entire Borel parameter region due to the truncation of contributions from the vacuum condensates with dimensions greater than 6. The following equation is employed to enhance the precision and rationality of the calculation of the result $\langle\xi^{\|;n}_{2;\phi}\rangle|_\mu$ [57]:

$$\langle\xi^{\|;n}_{2;\phi}\rangle|_\mu=\frac{\langle\xi^{\|;n}_{2;\phi}\rangle|_\mu\langle\xi^{\|;0}_{2;\phi}\rangle|_\mu|}{\sqrt{(\langle\xi^{\|;0}_{2;\phi}\rangle|_\mu)^2}}.\tag{11}$$

Here the squared zeroth-order moment $\langle\xi^{\|;n}_{2;\phi}\rangle|_\mu$ in the denominator is obtained by taking $n\to 0$ in Eq. (9), and its detailed expression is given by

$$\begin{aligned}(\langle\xi^{\|;0}_{2;\phi}\rangle|_\mu)^2=&\frac{e^{m_\phi^2/M^2}}{(f^{\|}_\phi)^2}\int_{4m_s^2}^{s_\phi}\mathrm{d}s e^{-s/M^2}\frac{v}{8\pi^2}(3-v^2)+\frac{2m_s\langle\bar{s}s\rangle}{M^4}+\frac{\langle\alpha_s G^2\rangle}{12\pi M^4}-\frac{m_s\langle g_s\bar{s}\sigma TGs\rangle}{9M^6}+\frac{4\langle g_s\bar{s}s\rangle}{81M^6}+\frac{\sum\langle g_s^2\bar{q}q\rangle^2}{486\pi^2M^6}\\&\times\left[-50\left(-\ln\frac{M^2}{\mu^2}\right)+105\right]+m_s^2\left\{\frac{\langle\alpha_s G^2\rangle}{3\pi M^6}-\frac{\langle g_s^3fG^3\rangle}{72\pi^2M^8}-\frac{\sum\langle g_s^2q\bar{q}\rangle^2}{972\pi^2M^8}\left[8\left(-\ln\frac{M^2}{\mu^2}\right)+132\right]-\frac{4}{3}\frac{m_s\langle\bar{s}s\rangle}{M^6}\right.\\&\left.-\frac{m_s\langle g_s\bar{s}\sigma TGs\rangle}{3M^8}-\frac{4}{81}\frac{\langle g_s\bar{s}s\rangle^2}{M^8}\right\}.\end{aligned}\tag{12}$$

The moments $\langle\xi^{\|;n}_{2;\phi}\rangle|_\mu$ and the Gegenbauer moments $a^n_{2;\phi}(\mu)$ can be related via the following equations [58]:

$$\langle\xi^{\|;2}_{2;\phi}\rangle|_\mu=\frac{1}{5}+\frac{12}{35}a^2_{2;\phi}(\mu),\tag{13}$$

$$\langle\xi^{\|;4}_{2;\phi}\rangle|_\mu=\frac{3}{35}+\frac{8}{35}a^2_{2;\phi}(\mu)+\frac{8}{77}a^4_{2;\phi}(\mu),\tag{14}$$

$$\langle\xi^{\|;6}_{2;\phi}\rangle|_\mu=\frac{1}{21}+\frac{12}{77}a^2_{2;\phi}(\mu)+\frac{120}{1001}a^4_{2;\phi}(\mu)+\frac{64}{2145}a^6_{2;\phi}(\mu),\quad\ldots.\tag{15}$$

B. The ϕ-meson longitudinal leading-twist LCDA from the LCHO model

The LCHO model is based on the BHL prescription and the Melosh-Wigner transformation, where the Melosh-Wigner transformation relates the light-cone spin state to the ordinary instant-form spin state wave functions and is one of the most important ingredients of the light-cone formalism [59]. In this context, we can construct a light-cone wave function for the quark-antiquark Fock state in the light-cone quark model by using the Melosh-Wigner rotation [60]. The complete light-front wave function is accomplished by appraising the spin and momentum space wave functions $\chi^{\Lambda}_{\lambda_1,\lambda_2}(x,\mathbf{k}_\perp)$ and $\psi^{\mathrm{R}}_{2;\phi}(x,\mathbf{k}_\perp)$, e.g.,

$$\Psi^{\|}_{2;\phi}(x,\mathbf{k}_\perp)=\chi^{\Lambda}_{\lambda_1,\lambda_2}(x,\mathbf{k}_\perp)\psi^{\mathrm{R}}_{2;\phi}(x,\mathbf{k}_\perp),\tag{16}$$

where $\chi^{\Lambda}_{\lambda_1,\lambda_2}(x,\mathbf{k}_\perp)$ depends on the ϕ-meson spin projection. The Fock expansion of the two-particle Fock state for the ϕ-meson includes two different types of spin configurations: longitudinal (L) and transverse (T), each with distinct λ_1 and λ_2. Here λ_1 and λ_2 represent the helicities of the quark and antiquark, respectively. Within the light-front holographic model, the Lorentz-invariant spin structure of vector mesons is expressed as [61]

$$\chi^{\mathrm{L(T)}}_{\lambda_1,\lambda_2}(x,\mathbf{k}_\perp)=\frac{\bar{u}_{\lambda_1}(k^+,\mathbf{k}_\perp)}{\sqrt{x}}(\epsilon_\Lambda\cdot\gamma)\frac{\nu_{\lambda_2}(k'^+,\mathbf{k}'_\perp)}{\sqrt{1-x}},\tag{17}$$

where ϵ_Λ is the polarization vector, and k and k' stand for the 4-momenta of the quark and the antiquark, respectively. The longitudinal and transverse polarizations of vector mesons are given by

$$\epsilon_{\mathrm{L}}=\left(\frac{P^+}{M_V},-\frac{M_V}{P^+},0,0\right)\quad\epsilon^{\mp}_{\mathrm{T}}=\mp\frac{1}{\sqrt{2}}(0,0,1,\pm i),\tag{18}$$

where P is the meson momentum and M_V is the mass of the vector meson. The spin wave functions of the pseudoscalar meson and vector meson are derived from the light-front holographic model [61] and the light-cone quark model [62,63]. The spin part of the wave function is determined by the Melosh-Wigner method, which establishes a connection between spin states transforming from the instanton form to the light-front form. For the case of $\Lambda = \mathrm{L}$, the spin part of the wave function for the ϕ-meson reads [61]

$$\chi^{\mathrm{L}}_{+,+}(x,\mathbf{k}_\perp) = +\frac{(1-2x)\mathcal{M}(k_x - ik_y)}{(\mathcal{M}+2m_s)\sqrt{2(\mathbf{k}_\perp^2+m_s)}}, \tag{19}$$

$$\chi^{\mathrm{L}}_{+,-}(x,\mathbf{k}_\perp) = +\frac{m_s(\mathcal{M}+2m_s)+2\mathbf{k}_\perp^2}{(\mathcal{M}+2m_s)\sqrt{2(\mathbf{k}_\perp^2+m_s)}}, \tag{20}$$

$$\chi^{\mathrm{L}}_{-,+}(x,\mathbf{k}_\perp) = +\frac{m_s(\mathcal{M}+2m_s)+2\mathbf{k}_\perp^2}{(\mathcal{M}+2m_s)\sqrt{2(\mathbf{k}_\perp^2+m_s)}}, \tag{21}$$

$$\chi^{\mathrm{L}}_{-,-}(x,\mathbf{k}_\perp) = -\frac{(1-2x)\mathcal{M}(k_x + ik_y)}{(\mathcal{M}+2m_s)\sqrt{2(\mathbf{k}_\perp^2+m_s)}}, \tag{22}$$

where m_s is the mass of the constitute s quark in the ϕ meson and the abbreviation $\bar{x} = (1-x)$ is used. This treatment agrees with the cases of ρ meson due to the same vector meson spin projection [64]. In the present paper, our main concern is the longitudinal distribution amplitude of the vector meson. Thus, we only need to consider the following spin part of the wave function that gives sizable contribution to the present case:

$$\chi_{2;\phi}(x,\mathbf{k}_\perp) = \frac{m_s(\mathcal{M}+2m_s)+2\mathbf{k}_\perp^2}{(\mathcal{M}+2m_s)\sqrt{2(\mathbf{k}_\perp^2+m_s)}}, \tag{23}$$

where $\mathcal{M} = \sqrt{(\mathbf{k}_\perp^2+m_s^2)/(x\bar{x})}$ is the invariant mass of the composite system. According to the BHL prescription, the momentum space wave function of the ϕ meson is [65]

$$\psi^{\mathrm{R}}_{2;\phi}(x,\mathbf{k}_\perp) = A^{\parallel}_{2;\phi}\varphi^{\parallel}_{2;\phi}(x)\exp\left[-\frac{1}{8\beta^2_{2;\phi}}\left(\frac{\mathbf{k}_\perp^2+m_s^2}{x\bar{x}}\right)\right], \tag{24}$$

where $A^{\parallel}_{2;\phi}$ is the normalization constant, whose value is primarily calculated by normalizing the wave function. $\beta_{2;\phi}$ is the harmonic parameter and determines the LCWF transverse behavior. The function $\varphi^{\parallel}_{2;\phi}(x)$ dominates the longitudinal distribution of the LCDA, which can be expressed in the following two formulations [66]:

$$\varphi^{\parallel(\mathrm{I})}_{2;\phi}(x) = 1 + b^2_{2;\phi}C_2^{3/2}(2x-1) + b^4_{2;\phi}C_4^{3/2}(2x-1), \tag{25}$$

$$\varphi^{\parallel(\mathrm{II})}_{2;\phi}(x) = (x\bar{x})^{\alpha_{2;\phi}}[1 + B^2_{2;\phi}C_2^{3/2}(2x-1)]. \tag{26}$$

The first one, denoted as $\varphi^{\parallel(\mathrm{I})}_{2;\phi}(x)$, adopts the usual Gegenbauer expansion. Its model parameters $b^2_{2;\phi}$ and $b^4_{2;\phi}$ can be fixed by using the nth-order Gegenbauer moments $a^n_{2;\phi}(\mu)$ that have been defined in Eq. (2). To derive a more accurate representation of $\phi^{\parallel}_{2;\phi}(x,\mu)$, it is necessary to increase the precision of the higher-order Gegenbauer polynomial. This treatment is discussed in detail in Ref. [67]. However, due to large coefficients that exist between $\langle\xi^{n;\parallel}_{2;\phi}\rangle|_\mu$ and $a^n_{2;\phi}(\mu)$, the reliability of calculating $a^n_{2;\phi}(\mu)$ using the QCD SR will decrease with the increment of the nth-order. Thus, we will also adopt another model, namely, $\varphi^{\parallel(\mathrm{II})}_{2;\phi}(x)$, to enhance the form of $\phi^{\parallel}_{2;\phi}(x,\mu)$, whose longitudinal part explicitly contains a factor $(x\bar{x})^{\alpha_{2;\phi}}$ that is close to the asymptotic form $\phi^{\parallel}_{2;\phi}(x,\mu\to\infty) = 6x\bar{x}$ [68].

By combining the spin and space wave functions, one can obtain the comprehensive wave function of the ϕ meson, i.e.,

$$\Psi^{\parallel}_{2;\phi}(x,\mathbf{k}_\perp) = A^{\parallel}_{2;\phi}\varphi^{\parallel}_{2;\phi}(x)\frac{m_s(\mathcal{M}+2m_s)+2\mathbf{k}_\perp^2}{(\mathcal{M}+2m_s)\sqrt{2(\mathbf{k}_\perp^2+m_s)}} \times\exp\left[-\frac{1}{8\beta^2_{2;\phi}}\left(\frac{\mathbf{k}_\perp^2+m_s^2}{x\bar{x}}\right)\right]. \tag{27}$$

By utilizing the relationship between the ϕ-meson leading-twist LCDA and the wave function, one can then derive the expression for the ϕ-meson longitudinal leading-twist LCDA,

$$\phi^{\parallel}_{2;\phi}(x,\mu) = \frac{2\sqrt{6}}{f^{\parallel}_\phi}\int_{|\mathbf{k}_\perp^2|\le\mu^2}\frac{\mathrm{d}^2\mathbf{k}_\perp}{16\pi^3}A^{\parallel}_{2;\phi}\varphi^{\parallel}_{2;\phi}(x) \times\frac{m_s(\mathcal{M}+2m_s)+2\mathbf{k}_\perp^2}{(\mathcal{M}+2m_s)\sqrt{2(\mathbf{k}_\perp^2+m_s)}} \times\exp\left[-\frac{1}{8\beta^2_{2;\phi}}\left(\frac{\mathbf{k}_\perp^2+m_s^2}{x\bar{x}}\right)\right]. \tag{28}$$

The next step is to determine the four model-dependent parameters. For $A^{\parallel}_{2;\phi}$ and $\beta_{2;\phi}$, they can be constrained by the following two conditions:

(i) The normalization of the wave function,

$$\int_0^1\mathrm{d}x\int\frac{\mathrm{d}^2\mathbf{k}_\perp}{16\pi^3}\Psi^{\parallel}_{2;\phi}(x,\mathbf{k}_\perp) = \frac{f^{\parallel}_\phi}{2\sqrt{6}}. \tag{29}$$

(ii) The probability of finding the lowest Fock state $|s\bar{s}\rangle$ in the ϕ-meson expansion,

$$P_\phi = \int_0^1\mathrm{d}x\int\frac{\mathrm{d}^2\mathbf{k}_\perp}{16\pi^3}|\Psi^{\parallel}_{2;\phi}(x,\mathbf{k}_\perp)|^2. \tag{30}$$

In this paper, the probability value is chosen as $P_\phi \approx 0.6$, mainly relying on the prediction for the K meson $P_K \approx 0.52$ as proposed by Guo and Huang [65]. Subsequently, the remaining two parameters, $\alpha_{2;\phi}$ and $B^2_{2;\phi}$ for $\varphi^{\|(\mathrm{II})}_{2;\phi}(x)$, can be fitted by equating its ξ moments $\langle \xi^{\|;n}_{2;\phi} \rangle|_\mu$ to the derived values give by the QCD sum rules (9). To make their values more accurately, we shall adopt the ξ moments up to tenth-order level.

C. The $D_s^+ \to \phi \ell^+ \nu_\ell$ semileptonic decay width

In the standard model, the matrix element for the semileptonic decay $D_s^+ \to \phi \ell^+ \nu_\ell$ can be written as

$$\mathcal{M}(D_s^+ \to \phi \ell^+ \nu_\ell) = \frac{G_F}{\sqrt{2}} V_{cs} H^\mu L_\mu, \tag{31}$$

where $G_F = 1.1663787(6) \times 10^{-5}\ \mathrm{GeV}^{-2}$ is the Fermi constant and V_{cs} is the Cabibbo-Kobayashi-Maskawa (CKM) matrix element for the weak transition $c \to s$. H^μ and L_μ represent the hadronic transition matrix element and the leptonic current, respectively, which are defined as follows:

$$\begin{aligned} H^\mu &= \langle \phi | V^\mu - A^\mu | D_s^+ \rangle, \\ L_\mu &= \bar{\nu}_\ell \gamma_\mu (1 - \gamma_5) \ell^+, \end{aligned} \tag{32}$$

where $V^\mu = (\bar{q} \gamma^\mu c)$ and $A^\mu = (\bar{q} \gamma^\mu \gamma_5 c)$ stand for the flavor-changing vector and axial-vector currents, respectively. The leptonic part has a simple structure that can be easily calculated using the lepton spinors. The transition between different hadrons is related to bound state effects and hadronization, which has nonperturbation mechanical characteristics. So the hadronic part is much more complicated and requires proper nonperturbative treatment within the QCD theory.

The hadronic matrix element comprises four vectors involved in the transition, namely, the four momentum and polarization vectors of the meson, which can be commonly expressed as various parameterized TFFs. More explicitly, the hadronic matrix element for $D_s^+ \to \phi$ can be parameterized in terms of five TFFs as follows [69]:

$$\begin{aligned} &\langle \phi(p,\lambda) | \bar{s} \gamma_\mu (1 - \gamma_5) c | D_s^+(p+q) \rangle \\ &= -i e^{*(\lambda)}_\mu (m_{D_s^+} + m_\phi) A_1(q^2) \\ &\quad + i(2p+q)_\mu \frac{e^{*(\lambda)} \cdot q}{m_{D_s^+} + m_\phi} A_2(q^2) \\ &\quad + i q_\mu (e^{*(\lambda)} \cdot q) \frac{2 m_\phi}{q^2} [A_3(q^2) - A_0(q^2)] \\ &\quad - \epsilon^{\mu\nu\alpha\beta} e^{*(\lambda)}_\nu q_\alpha p_\beta \frac{2V(q^2)}{m_{D_s^+} + m_\phi}, \end{aligned} \tag{33}$$

where $m_{D_s^+}$ and m_ϕ are masses of D_s^+ and ϕ, respectively, $p = p_\phi$ is the ϕ-meson momentum, $q = (p_{D_s^+} - p_\phi)$ is the momentum transfer, and $e^{*(\lambda)}$ stands for the polarization vector of the ϕ meson with $\lambda = (\perp, \|)$, representing its transverse or longitudinal component, respectively. The TFFs $A_1(q^2)$ and $A_2(q^2)$ are associated with the exchange of a particle with quantum state $J^P = 1^+$, while the TFF $V(q^2)$ is associated with $J^P = 1^-$ [70,71]. The TFF $A_3(q^2)$ is not independent, which can be expressed as a linear relation of $A_1(q^2)$ and $A_2(q^2)$, i.e.,

$$A_3(q^2) = \frac{(m_{D_s^+} + m_\phi)}{2m_\phi} A_1(q^2) - \frac{(m_{D_s^+} - m_\phi)}{2m_\phi} A_2(q^2). \tag{34}$$

The problem of calculating the decay distribution aside, the obtained $D_s^+ \to \phi$ TFFs are also linked to the crucial angle variables and provide helpful information to determine their magnitudes. All the final state particles, excluding the neutrino, can be reconstructed with relatively high efficiency. Four independent kinematic variables characterize the semileptonic decay $D_s^+ \to \phi \ell^+ \nu_\ell$, wherein the ϕ meson will subsequently decay into two pseudoscalar mesons such as K^+K^-. The common choices of the four variables are q^2 and the three angles θ_ℓ, θ_K, and χ shown in Fig. 1, respectively. The polar angle θ_ℓ stands for the angle between the momentum of the charged lepton in the rest frame of the intermediate W^+ boson and the direction opposite to the momentum of the final ϕ meson in the rest frame of the D_s^+ meson. θ_K is the angle between the momentum of the K^+ meson and the center-of-mass momentum of the K^+K^- pair. χ is the angle between the two planes defined by the $(\ell^+\nu_\ell)$ and (K^+K^-) pairs, respectively.

To calculate the differential decay rate for the channel $D_s^+ \to \phi \ell^+ \nu_\ell$, it is convenient to express the hadronic matrix element by the helicity amplitudes $H_{\pm,0,t}$. Those helicity amplitudes are Lorentz-invariant functions which can be formally expressed as the linear combination of the TFFs as follows:

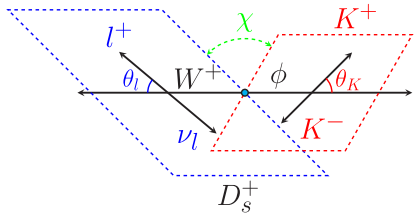

FIG. 1. The diagram that illustrates the angular configurations utilized in the calculation of the differential rate for the process $D_s^+ \to \phi \ell^+ \nu_\ell$. The momenta of $\ell^+\nu_\ell$ are depicted in the rest frame of the virtual W^+ boson, while those of K^+K^- are represented in the rest frame of the ϕ meson.

$$H_{\pm}(q^2) = \frac{\lambda^{1/2}(m_{D_s^+}^2, m_\phi^2, q^2)}{m_{D_s^+}+m_\phi}\left[\frac{(m_{D_s^+}+m_\phi)^2}{\lambda^{1/2}(m_{D_s^+}^2, m_\phi^2, q^2)}A_1(q^2) \mp V(q^2)\right],$$
$$H_0(q^2) = \frac{1}{2m_\phi\sqrt{q^2}}\left[(m_{D_s^+}+m_\phi)(m_{D_s^+}^2 - m_\phi^2 - q^2)A_1(q^2) - \frac{\lambda(m_{D_s^+}^2, m_\phi^2, q^2)}{m_{D_s^+}+m_\phi}A_2(q^2)\right],$$
$$H_t(q^2) = \frac{\lambda^{1/2}(m_{D_s^+}^2, m_\phi^2, q^2)}{\sqrt{q^2}}A_0(q^2). \quad (35)$$

The main difference between the helicity amplitudes and the usual TFFs lies in the method of decomposition. The γ structures of the hadronic matrix elements can be decomposed into Lorentz-invariant structures by using covariant decomposition for the TFFs decomposition method, while the helicity amplitude decomposition method uses the polarization vector of the off-shell W^+ boson to obtain a newly combined Lorentz-invariant structure. The use of helicity amplitudes have some advantages in comparison to the usual treatment of TFFs [72–75]: (I) Dispersive bounds on the helicity amplitudes parameterization can be achieved via the diagonalizable unitarity relations. (II) The polarized decay widths of $D_s^+ \to \phi$ can be well studied by using the helicity amplitudes. (III) Since the helicity amplitudes have a definite spin-parity quantum number, it is convenient to consider the contribution of the excited state of the meson in the transition process. (IV) The polarization and asymmetry parameters of $D_s^+ \to \phi$ can be accurately determined through the utilization of helicity amplitudes.

By using the helicity amplitudes, the differential decay rate for $D_s^+ \to \phi\ell^+\nu_\ell$ with the cascade decay $\phi \to K^+K^-$ can be expressed in terms of the above suggested four kinematic variables as q^2, θ_ℓ, θ_K, and χ [24], e.g.,

$$\frac{d\Gamma(D_s^+ \to \phi\ell^+\nu_\ell, \phi \to K^+K^-)}{dq^2 d\cos\theta_K d\cos\theta_\ell d\chi} = \frac{3}{8(4\pi)^4}G_F^2|V_{cs}|^2\frac{|\mathbf{p_2}|m_\ell^2}{m_{D_s^+}^2}\mathcal{B}(\phi \to K^+K^-)\{\sin^2\theta_K\sin^2\theta_\ell|H_+(q^2)|^2 + \sin^2\theta_K\sin^2\theta_\ell|H_-(q^2)|^2 + 4\cos^2\theta_K\cos^2\theta_\ell|H_0(q^2)|^2 + 4\cos^2\theta_K|H_t(q^2)|^2 + \sin^2\theta_K\sin^2\theta_\ell\cos 2\chi H_+(q^2)H_-(q^2) + \sin 2\theta_K\sin 2\theta_\ell\cos 2\chi H_+(q^2)H_0(q^2) + \sin 2\theta_K\sin 2\theta_\ell\cos 2\chi H_-(q^2)H_0(q^2) + 2\sin 2\theta_K\sin\theta_\ell\cos\chi H_+(q^2)H_t(q^2) + 2\sin 2\theta_K\sin\theta_\ell\cos\chi H_-(q^2)H_t(q^2) + 8\cos^2\theta_K\cos\theta_\ell H_0(q^2)H_t(q^2)\}, \quad (36)$$

where $|\mathbf{p_2}| = \lambda^{1/2}(m_{D_s^+}^2, m_\phi^2, q^2)/(2m_{D_s^+})$ represents the magnitude of the **3**-momentum of the daughter meson in the rest frame of D_s^+, and $\lambda(x,y,z) = (x+y-z)^2 - 4xy$ is the Källen function. The helicities of the vector meson ϕ and the W^+ boson must be identical due to the spin-zero nature of the parent meson. The amplitudes for the helicities 0, +1, and −1 are proportional to $H_0(q^2)$, $H_+(q^2)$, and $H_-(q^2)$, respectively. Additionally, $H_t(q^2)$ is proportional to $1/\sqrt{q^2}$ and is most significant at the low q^2 region. The detailed dynamics of the hadronic current is described by the variation of these helicity amplitudes with q^2. To obtain the distribution of the polar angle θ_ℓ, one can integrate Eq. (36) over the angle θ_K and the azimuthal angle χ. Detailed processes for the integration can be found in Ref. [17]. The resultant differential decay width over q^2 and $\cos\theta_\ell$ can be expressed as [27]

$$\frac{d\Gamma(D_s^+ \to \phi\ell^+\nu_\ell)}{dq^2 d\cos\theta_\ell} = \frac{G_F^2|V_{cs}|^2}{64(2\pi)^3 m_{D_s^+}^3}\lambda^{1/2}(m_{D_s^+}^2, m_\phi^2, q^2)\frac{(q^2-m_\ell^2)^2}{q^2}\left[(1+\cos\theta_\ell)\mathcal{H}_U + 2\sin^2\theta_\ell\mathcal{H}_L + 2\cos\theta_\ell\mathcal{H}_P + \frac{m_\ell^2}{q^2}(\sin^2\theta_\ell\mathcal{H}_U + 2\cos^2\theta_\ell\mathcal{H}_L + 2\mathcal{H}_S - 4\cos\theta_\ell\mathcal{H}_{SL})\right], \quad (37)$$

where the m_ℓ with $\ell = (e,\mu)$ is the lepton mass and the helicity structure functions $\mathcal{H}_i$ are defined as

$$\mathcal{H}_U = |H_+|^2 + |H_-|^2,\ \mathcal{H}_L = |H_0|^2,\ \mathcal{H}_P = |H_+|^2 - |H_-|^2,\ \mathcal{H}_{SL} = \mathrm{Re}(H_0H_t^\dagger),\ \mathcal{H}_S = |H_t|^2. \quad (38)$$

Based on the helicity amplitudes described above, the forward-backward asymmetry $A_{FB}^\ell(q^2)$, lepton-side convexity parameter $C_F^\ell(q^2)$, and the longitudinal (transverse) polarization of the final charged lepton $P_{L(T)}^\ell(q^2)$, as well as the longitudinal (transverse) polarization fraction of the final ϕ-meson $F_{L(T)}^\ell(q^2)$ in the semileptonic decay $D_s^+ \to \phi\ell^+\nu_\ell$, are expressed as follows [27]:

$$A_{FB}^\ell(q^2) = \frac{3}{4}\frac{\mathcal{H}_P - 2\delta\mathcal{H}_{SL}}{\mathcal{H}_{total}}, \quad (39)$$

$$C_{\rm F}^{\ell}(q^2)=\frac{3}{4}(1-\delta)\frac{\mathcal{H}_{\rm U}-2\mathcal{H}_{\rm L}}{\mathcal{H}_{\rm total}}, \tag{40}$$

$$P_{\rm L}^{\ell}(q^2)=\frac{(\mathcal{H}_{\rm U}+\mathcal{H}_{\rm L})(1-\frac{\delta}{2})-\frac{3\delta}{2}\mathcal{H}_{\rm S}}{\mathcal{H}_{\rm total}}, \tag{41}$$

$$P_{\rm T}^{\ell}(q^2)=-\frac{3\pi m_{\ell}}{8\sqrt{q^2}}\frac{\mathcal{H}_{\rm P}+2\mathcal{H}_{\rm SL}}{\mathcal{H}_{\rm total}}, \tag{42}$$

$$F_{\rm L}^{\ell}(q^2)=\frac{\mathcal{H}_{\rm L}(1+\frac{\delta}{2})+\frac{3\delta}{2}\mathcal{H}_{\rm S}}{\mathcal{H}_{\rm total}}. \tag{43}$$

Here, the total helicity amplitude takes the form $\mathcal{H}_{\rm total}=(\mathcal{H}_{\rm U}+\mathcal{H}_{\rm L})(1+\delta/2)+3\delta\mathcal{H}_{\rm S}/2$ with $\delta=m_{\ell}^2/q^2$ and $F_T^{\ell}(q^2)=1-F_L^{\ell}(q^2)$. In this paper, the lepton is considered as $\ell=(e,\mu)$ and thus the leptonic mass can be neglected due to chiral suppression. Subsequently, the differential decay width for $D_s^+\to\phi\ell^+\nu_{\ell}$ can be written as [13,76,77]

$$\begin{aligned}\frac{{\rm d}\Gamma(D_s^+\to\phi\ell^+\nu_{\ell})}{{\rm d}q^2}&=\frac{G_F^2|V_{\rm cs}|^2}{192\pi^3m_{D_s^+}^3}\lambda^{1/2}(m_{D_s^+}^2,m_{\phi}^2,q^2)q^2\\&\times[|H_+|^2+|H_-|^2+|H_0|^2]\\&=\frac{{\rm d}\Gamma_{\rm L}}{{\rm d}q^2}+\frac{{\rm d}\Gamma_{\rm T}^+}{{\rm d}q^2}+\frac{{\rm d}\Gamma_{\rm T}^-}{{\rm d}q^2}.\end{aligned} \tag{44}$$

The above formula indicates that there are three polarization states for the ϕ meson: one longitudinal state and two transverse polarization states (right- and left-handed). The differential decay width for the longitudinally polarized ϕ meson has the form

$$\begin{aligned}\frac{{\rm d}\Gamma_{\rm L}}{{\rm d}q^2}&=\frac{G_F^2|V_{\rm cs}|^2}{192\pi^2m_{D_s^+}^3}\lambda^{1/2}(m_{D_s^+}^2,m_{\phi}^2,q^2)q^2\left|\frac{1}{2m_{\phi}\sqrt{q^2}}\right.\\&\times\left[(m_{D_s^+}^2-m_{\phi}^2-q^2)(m_{D_s^+}^2+m_{\phi})A_1(q^2)\right.\\&\left.\left.-\frac{\lambda(m_{D_s^+}^2,m_{\phi}^2,q^2)}{m_{D_s^+}^2+m_{\phi}}A_2(q^2)\right]\right|^2,\end{aligned} \tag{45}$$

and for the transverse differential decay width, we have

$$\begin{aligned}\frac{{\rm d}\Gamma_{\rm T}^{\pm}}{{\rm d}q^2}&=\frac{G_F^2|V_{\rm cs}|^2}{192\pi^2m_{D_s^+}^3}\lambda^{1/2}(m_{D_s^+}^2,m_{\phi}^2,q^2)q^2\left|(m_{D_s^+}+m_{\phi})\right.\\&\left.\times A_1(q^2)\mp\frac{\lambda^{1/2}(m_{D_s^+}^2,m_{\phi}^2,q^2)}{(m_{D_s^+}+m_{\phi})}V(q^2)\right|^2.\end{aligned} \tag{46}$$

Here the symbols "+" and "−" denote the right- and left-handed states, respectively. The combined transverse and total decay widths are $\Gamma_{\rm T}=\Gamma_{\rm T}^+ +\Gamma_{\rm T}^-$ and $\Gamma=\Gamma_{\rm L}+\Gamma_{\rm T}$. After considering the D_s^+-meson lifetime and integration about the differential decay width, we can get the total branching fractions for $D_s^+\to\phi\ell^+\nu_{\ell}$.

D. The $D_s^+\to\phi$ TFFs within the LCSR approach

In this subsection, we adopt the LCSR approach to calculate the TFFs $A_0(q^2)$, $A_1(q^2)$, $A_2(q^2)$, and $V(q^2)$, which are associated with the current $\bar{s}(x)\gamma_{\mu}(1-\gamma_5)c(x)$ and have been defined in Eq. (33). We adopt the following correlation function (correlator) to derive the $D_s^+\to\phi$ TFFs:

$$\begin{aligned}\Pi_{\mu}(p,q)&=-i\int{\rm d}^4x e^{iq\cdot x}\langle\phi(p,\lambda)|T\{j_{\mu}(x),j_{D_s^+}^{\dagger}(0)\}|0\rangle\\&=\Pi_1 e_{\mu}^{*(\lambda)}-\Pi_2(e^{*(\lambda)}\cdot q)(2p+q)_{\mu}\\&\quad-\Pi_3(e^{*(\lambda)}\cdot q)q_{\mu}-i\Pi_V\epsilon_{\mu}^{\alpha\beta\gamma}e_{\alpha}^{*(\lambda)}q_{\beta}p_{\gamma},\end{aligned} \tag{47}$$

where $j_{\mu}(x)=\bar{s}(x)\gamma_{\mu}(1-\gamma_5)c(x)$ and $j_{D_s^+}^{\dagger}(x)=\bar{c}(x)\times(1-\gamma_5)s(x)$. To derive the LCSRs of the TFFs, we need to deal with the above correlator from two aspects. On the one hand, to deal with the correlator in the spacelike q^2 region, we can apply the operator product expansion to the right-hand side of Eq. (47) near the light cone $x^2\to 0$. The contributions to OPE can be obtained by contracting the quark fields to a full c-quark propagator. Processes for dealing with the OPE part is similar to the case of $B\to K^*$ TFFs, which have been given in Ref. [74]. The interested readers may turn to this reference for detailed calculation technology. Mainly, the matrix elements of the nonlocal operators between the vector ϕ meson and vacuum states can be arranged as the LCDAs with increasing twists, e.g., leading-twist, twist-3, twist-4 LCDAs, and so on. Contributions from the higher-twist LCDAs are generally power suppressed from the leading-twist one, which, however, may have sizable contributions in certain cases. In our present calculation, we will derive the LCSRs for the TFFs up to twist-4 accuracy, and up to twist-4 accuracy, we have

$$\begin{aligned}\langle 0|\bar{s}(0)\gamma_{\mu}s(x)|\phi(p,\lambda)\rangle&=m_{\phi}f_{\phi}^{\parallel}\left\{\frac{e^{*(\lambda)}\cdot x}{p\cdot x}p_{\mu}\int_0^1{\rm d}u e^{iup\cdot x}\right.\\&\times\left[\phi_{2;\phi}^{\parallel}(u)+\frac{m_{\phi}^2x^2}{16}\phi_{4;\phi}^{\parallel}(u)\right]\\&-\frac{1}{2}x_{\mu}\frac{e^{*(\lambda)}\cdot x}{(p\cdot x)^2}m_{\phi}^2\\&\times\int_0^1{\rm d}u e^{iup\cdot x}\bar{g}_3(u)\\&\left.+e_{\perp\mu}^{*(\lambda)}\int_0^1{\rm d}u e^{iup\cdot x}\phi_{3;\phi}^{\perp}(u)\right\},\end{aligned} \tag{48}$$

$$\langle 0|\bar{s}(0)\gamma_\mu\gamma_5 s(x)|\phi(p,\lambda)\rangle = -\frac{1}{4}m_\phi f_\phi^{\parallel}\varepsilon_{\mu\nu\alpha\beta}e_\nu^{*(\lambda)}p_\alpha x_\beta \times \int_0^1 \mathrm{d}u e^{iup\cdot x}\psi_{3;\phi}^{\perp}(u), \quad (49)$$

where $\bar{g}_3(u)$ is the combined function for short, e.g., $\bar{g}_3(u) = [\psi_{4;\phi}^{\parallel}(u) + \phi_{2;\phi}^{\parallel}(u) - 2\phi_{3;\phi}^{\perp}(u)]$. $\phi_{2;\phi}^{\parallel}(u)$ is the longitudinal leading-twist LCDA, $\phi_{3;\phi}^{\perp}(u)$ and $\psi_{3;\phi}^{\perp}(u)$ are twist-3 LCDAs, and $\phi_{4;\phi}^{\parallel}(u)$ and $\psi_{4;\phi}^{\parallel}(u)$ are twist-4 LCDAs, respectively. Contributions from those higher-twist LCDAs are generally power suppressed and we directly take the ones suggested in Refs. [37,78].

On the other hand, the correlator (47) in the timelike q^2 region can be treated with the hadronic representation, which is achieved by inserting a complete set of the intermediate states with the same quantum numbers in the correlator. By isolating the pole term of the lowest pseudoscalar D_s^+ meson, we obtain the following representation of the correlator from the hadron side:

$$\Pi_\mu(p,q) = \frac{\langle\phi|\bar{s}\gamma_\mu(1-\gamma_5)c|D_s^+\rangle\langle D_s^+|\bar{c}\gamma_5 s|0\rangle}{m_{D_s^+}^2 - (p+q)^2} + \sum_{\mathrm{H}}\frac{\langle\phi|\bar{s}\gamma_\mu(1-\gamma_5)c|D_s^{\mathrm{H}}\rangle\langle D_s^{\mathrm{H}}|\bar{c}(1-\gamma_5)s|0\rangle}{m_{D_s^{\mathrm{H}}}^2 - (p+q)^2}, \quad (50)$$

where $\langle D_s^+|\bar{c}\gamma_5 q|0\rangle = im_{D_s^+}^2 f_{D_s^+}/(m_c+m_s)$, and $f_{D_s^+}$ is the decay constant of the D_s^+ meson. To derive the invariant amplitudes $\Pi_{0,1,2,V}$ required in hadronic representation, we adopt the standard sum rule processes. By substituting the parameterization of the matrix elements (33) into (50), we obtain

$$\Pi_{0,1,2,V}^{\mathrm{had}}[q^2,(p+q)^2] = \frac{m_{D_s^+}^2 f_{D_s^+}}{m_c+m_s}\frac{1}{m_{D_s^+}^2-(p+q)^2} \times C_{0,1,2,V}A_{0,1,2,V}(q^2) + \cdots, \quad (51)$$

where the symbol "$\cdots$" represents the invariant amplitudes of the high resonance states and the continuum states. The coefficients $C_{0,1,2,V}$ take the values: $C_0 = -2m_\phi m_{D_s^+}^2 f_{D_s^+}/q^2$, $C_1 = m_{D_s^+}+m_\phi$, $C_2 = -1/(m_{D_s^+}+m_\phi)$, and $C_V = -2i/(m_{D_s^+}+m_\phi)$. Then we can write the invariant amplitudes $\Pi_{0,1,2,V}^{\mathrm{had}}$ using the general dispersion relation [35]

$$\Pi_{0,1,2,V}^{\mathrm{had}}[q^2,(p+q)^2] = \int_{t_{\min}}^{\infty}\frac{\rho_{0,1,2,V}(q^2,s)}{s-(p+q)^2}\mathrm{d}s, \quad (52)$$

where possible subtractions have been neglected, and the concrete expressions of the spectral density $\rho_{0,1,2,V}(q^2,s)$ are given as follows:

$$\rho_{0,1,2,V}(q^2,s) = \delta(s-m_{D_s^+}^2)\frac{m_{D_s^+}^2 f_{D_s^+}}{(m_c+m_s)}C_{0,1,2,V} \times A_{0,1,2,V}(q^2) + \rho_{0,1,2,V}^{\mathrm{H}}(q^2,s). \quad (53)$$

The second term in Eq. (53) corresponds to the spectral density of higher resonances and continuum states, which can be approximated by invoking the conventional quark-hadron duality ansatz [31]

$$\rho_{0,1,2,V}^{\mathrm{H}}(q^2,s) = \frac{1}{\pi}\mathrm{Im}\Pi_{0,1,2,V}^{\mathrm{OPE}}(q^2,s)\theta(s-s_0), \quad (54)$$

where s_0 is the threshold parameter and $\mathrm{Im}\Pi_{0,1,2,V}^{\mathrm{OPE}}(q^2,s)$ is obtained from the imaginary part of the correlator (47) calculated in the OPE. To suppress the contributions from the higher excited states and the continuum states, we apply the usual Borel transformation with respect to the dispersion integration (52),

$$\Pi_{0,1,2,V}[q^2,M^2] = \int_{t_{\min}}^{\infty}\rho_{0,1,2,V}(q^2,s)e^{-s/M^2}\mathrm{d}s, \quad (55)$$

where $t_{\min} = (m_c+m_s)^2$. With the help of Eqs. (53) and (54), we then obtain

$$\Pi_{0,1,2,V}[q^2,M^2] = \frac{m_{D_s^+}^2 f_{D_s^+}}{(m_c+m_s)}e^{-m_{D_s^+}^2/M^2}C_{0,1,2,V}A_{0,1,2,V}(q^2) + \frac{1}{\pi}\int_{s_0}^{\infty}\mathrm{Im}\Pi_{0,1,2,V}^{\mathrm{OPE}}(q^2,s)e^{-s/M^2}\mathrm{d}s. \quad (56)$$

Finally, by equating the correlators within different q^2 regions yield the desired LCSRs for the $D_s^+ \to \phi$ TFFs, e.g.,

$$A_1(q^2) = \frac{2m_c(m_c+m_s)m_\phi f_\phi^{\parallel}}{m_{D_s^+}^2(m_{D_s^+}+m_\phi)f_{D_s^+}}\left\{\int_{u_0}^1 \mathrm{d}u\exp\left(\frac{m_{D_s^+}^2-s(u)}{M^2}\right)\left(\frac{1}{u}\phi_{3;\phi}^{\perp}(u) - \frac{m_\phi^2}{u^2M^2}\bar{G}_3(u)\right) + m_\phi^2 \times \exp\left(\frac{m_{D_s^+}^2-s(u)}{M^2}\right)\frac{\bar{G}_3(u)}{q^2-m_c^2-u^2m_\phi^2}\Big|_{u\to u_0}\right\}, \quad (57)$$

$$A_2(q^2)=\frac{2m_c(m_c+m_s)(m_{D_s^+}+m_\phi)m_\phi f_\phi^\parallel}{m_{D_s^+}^2 f_{D_s^+}}\left\{\int_{u_0}^1\frac{\mathrm{d}u}{M^2}\exp\left(\frac{m_{D_s^+}^2-s(u)}{M^2}\right)\left(\frac{1}{u^2}\Phi_{2;\phi}^\parallel(u)+\frac{m_c^2m_\phi^2}{4u^4M^4}\Phi_{4;\phi}^\parallel(u)\right.\right.$$
$$-\frac{\Phi_{3;\phi}^\perp(u)}{u^2}+\frac{m_\phi^2}{u^2M^2}\bar{G}_3(u)\Big)+\exp\left(\frac{m_{D_s^+}^2-s(u)}{M^2}\right)\left[\frac{\Phi_{2;\phi}^\parallel(u)}{q^2-m_c^2-u^2m_\phi^2}m_c^2m_\phi^2\right.$$
$$+\left(\frac{m_c^2-q^2}{(q^2-m_c^2-u^2m_\phi^2)^5}(m_c^2-2u^2m_\phi^2-q^2)\Phi_{4;\phi}^\parallel(u)+\frac{u^3m_c^2m_\phi^4}{(q^2-m_c^2-u^2m_\phi^2)^4}\frac{d}{du}\Phi_{4;\phi}^\parallel(u)\right.$$
$$\left.-\frac{u^2m_c^2m_\phi^2}{4(q^2-m_c^2-u^2m_\phi^2)^3}\frac{d^2}{d^2u}\Phi_{4;\phi}^\parallel(u)\right)-\left(\frac{2u^3m_\phi^2}{(q^2-m_c^2-u^2m_\phi^2)^3}\bar{G}_3(u)+\frac{u^2}{(q^2-m_c^2-u^2m_\phi^2)^2}\frac{d}{du}\bar{G}_3(u)\right)$$
$$\left.\left.+\frac{\Phi_{3;\phi}^\perp(u)}{q^2-m_c^2-u^2m_\phi^2}\right]\right|_{u\to u_0}\Bigg\}, \tag{58}$$

$$A_0(q^2)=A_3(q^2)+\frac{q^2m_c(m_c+m_s)m_\phi f_\phi^\parallel}{m_{D_s^+}^2 f_{D_s^+}}\left\{\int_{u_0}^1\frac{\mathrm{d}u}{M^2}\exp\left(\frac{m_{D_s^+}^2-s(u)}{M^2}\right)\left(\frac{1}{u^2}\Phi_{2;\phi}^\parallel(u)-\frac{m_c^2m_\phi^2}{4u^4M^4}\Phi_{4;\phi}^\parallel(u)\right.\right.$$
$$-\frac{\Phi_{3;\phi}^\perp(u)}{u^2}-\frac{(2-u)m_\phi^2}{u^2M^2}\bar{G}_3(u)\Big)+\exp\left(\frac{m_{D_s^+}^2-s(u)}{M^2}\right)\left[\frac{1}{q^2-m_c^2-u^2m_\phi^2}\Phi_{2;\phi}^\parallel(u)\right.$$
$$+\left(\frac{m_c^2-q^2}{(q^2-m_c^2-u^2m_\phi^2)^5}m_c^2m_\phi^2(m_c^2-2u^2m_\phi^2-q^2)\Phi_{4;\phi}^\parallel(u)+\frac{u^3m_c^2m_\phi^4}{(q^2-m_c^2-u^2m_\phi^2)^4}\frac{d}{du}\Phi_{4;\phi}^\parallel(u)\right.$$
$$-\frac{u^2m_c^2m_\phi^2}{4(q^2-m_c^2-u^2m_\phi^2)^3}\frac{d^2}{d^2u}\Phi_{4;\phi}^\parallel(u)\Big)+\left(2\frac{(m_c^2+3u^2m_\phi^2-q^2)-u^3m_\phi^2}{(q^2-m_c^2-u^2m_\phi^2)^3}\bar{G}_3(u)+u(2-u)\right.$$
$$\left.\left.\left.\times\frac{1}{(q^2-m_c^2-u^2m_\phi^2)^2}\frac{d}{du}\bar{G}_3(u)\right)+\frac{\Phi_{3;\phi}^\perp(u)}{q^2-m_c^2-u^2m_\phi^2}\right]\right|_{u\to u_0}\Bigg\}, \tag{59}$$

$$V(q^2)=\frac{m_c(m_c+m_s)(m_{D_s^+}+m_\phi)m_\phi f_\phi^\parallel}{2m_{D_s^+}^2 f_{D_s^+}}\left\{\int_{u_0}^1\mathrm{d}u\exp\left(\frac{m_{D_s^+}^2-s(u)}{M^2}\right)\frac{\psi_{3;\phi}^\perp(u)}{u^2M^2}-\exp\left(\frac{m_{D_s^+}^2-s(u)}{M^2}\right)\right.$$
$$\left.\left.\times\frac{1}{q^2-m_c^2-u^2m_\phi^2}\psi_{3;\phi}^\perp(u)\right|_{u\to u_0}\right\}, \tag{60}$$

where $s(u)=[m_c^2-\bar{u}(q^2-um_\phi^2)]/u$ and $u_0=(q^2-s_0+m_\phi^2+\sqrt{(q^2-s_0+m_\phi^2)^2-4m_\phi^2(q^2-m_c^2)})/(2m_\phi^2)$ with $\bar{u}=1-u$. Here, two simplified distribution amplitudes (DAs) are defined as

$$\Phi_{2;\phi}^\parallel(u)=\int_0^u\mathrm{d}v\phi_{2;\phi}^\parallel(u), \tag{61}$$

$$\bar{G}_3(u)=\int_0^u\mathrm{d}v\int_0^v\mathrm{d}w\bar{g}_3(w). \tag{62}$$

The helicity amplitudes $H_{\pm,0,t}$ and the total and differential decay widths can be calculated once the above TFFs have been determined.

III. NUMERICAL RESULTS AND DISCUSSIONS

A. Input parameters

To do the numerical analysis on the properties of ϕ-meson longitudinal leading-twist LCDA and $D_s^+\to\phi$ TFFs, the values of parameters are taken as follows. The ϕ-meson mass and decay constant are $m_\phi=1.019$ and $f_\phi^\parallel=0.231\pm0.004$ GeV [37], respectively. The charm-quark current mass $m_c(\bar{m}_c)=1.27\pm0.02$ GeV, the s-quark current mass $m_s(2\ \mathrm{GeV})=0.093^{+0.011}_{-0.005}$ GeV, and the D_s^+-meson mass and decay constant are $m_{D_s^+}=1.968$ [79] and $f_{D_s^+}=0.256\pm0.004$ GeV [80]. When calculating the moments of the distributed amplitude, we also need to know the values of nonperturbative vacuum condensates up to six dimensions, which can be read from Ref. [66]. The renormalization scale is set as $\mu_k=(m_{D_s^+}^2-\bar{m}_c^2)^{1/2}\approx1.5$ GeV.

Furthermore, we also need to know the values of the nonperturbative vacuum condensates up to dimension six [66],

$$\begin{aligned}
\langle s\bar{s}\rangle &= (-1.789^{+0.168}_{-0.084})\times 10^{-2}\ \text{GeV}^3,\\
\langle g_s\bar{q}q\rangle^2 &= (2.082^{+0.734}_{-0.697})\times 10^{-3}\ \text{GeV}^6,\\
\langle g_s\bar{s}\sigma TGs\rangle &= (-1.431^{+0.139}_{-0.076})\times 10^{-2}\ \text{GeV}^5,\\
\langle g_s^2\bar{q}q\rangle^2 &= (7.420^{+2.614}_{-2.483})\times 10^{-3}\ \text{GeV}^6,\\
\langle \alpha_s G^2\rangle &= 0.038\pm 0.011\ \text{GeV}^4,\\
\langle g_s^3 fG^3\rangle &\approx 0.045\ \text{GeV}^6,\\
\sum\langle g_s^2\bar{q}q\rangle^2 &= (1.891^{+0.665}_{-0.633})\times 10^{-2}\ \text{GeV}^6.
\end{aligned} \tag{63}$$

The ratio $\kappa=\langle s\bar{s}\rangle/\langle q\bar{q}\rangle=0.74\pm 0.03$ is given in Ref. [81]. To ensure the consistency of the calculation, all vacuum condensates and quark masses should be evolved from some hadronic scale μ_0 that is of order $\mathcal{O}(1\ \text{GeV})$ to the required renormalization scale by using the renormalization group equation, e.g., [82–85],

$$\begin{aligned}
\bar{m}_s(\mu) &= \bar{m}_s(\mu_0)\left[\frac{\alpha_s(\mu_0)}{\alpha_s(\mu)}\right]^{4/\beta_0},\\
\langle q\bar{q}\rangle(\mu) &= \langle q\bar{q}\rangle(\mu_0)\left[\frac{\alpha_s(\mu_0)}{\alpha_s(\mu)}\right]^{-4/\beta_0},\\
\langle g_s\bar{q}q\rangle^2(\mu) &= \langle g_s\bar{q}q\rangle^2\left[\frac{\alpha_s(\mu_0)}{\alpha_s(\mu)}\right]^{-2/(3\beta_0)},\\
\langle g_s\bar{q}\sigma TGq\rangle(\mu) &= \langle g_s\bar{q}\sigma TGq\rangle(\mu_0)\left[\frac{\alpha_s(\mu_0)}{\alpha_s(\mu)}\right]^{-2/(3\beta_0)},\\
\langle g_s^2\bar{q}q\rangle^2(\mu) &= \langle g_s^2\bar{q}q\rangle^2(\mu_0),\\
\langle \alpha_s G^2\rangle(\mu) &= \langle \alpha_s G^2\rangle(\mu_0),\\
\langle g_s^3 fG^3\rangle(\mu) &= \langle g_s^3 fG^3\rangle(\mu_0).
\end{aligned} \tag{64}$$

Additionally, the evolution equation of the Gegenbauer moments is

$$a^n_{2;\phi}(\mu)=a^n_{2;\phi}(\mu_0)\left[\frac{\alpha_s(\mu)}{\alpha_s(\mu_0)}\right]^{\gamma_n/2\beta_0}, \tag{65}$$

where $\beta_0=11-2/3n_f$, with n_f being the number of active flavors. The one-loop anomalous dimension γ_n can be expressed in two ways: longitudinal $\gamma_n^{\parallel}$ and transverse $\gamma_n^{\perp}$. In the context, we primarily utilize the longitudinal one-loop anomalous dimension to satisfy the following equation [37]:

$$\gamma_n^{\parallel}=8C_F\left[\psi(n+2)+\gamma_E-\frac{3}{4}-\frac{1}{2(n+1)(n+2)}\right], \tag{66}$$

where $C_F=4/3$. Using Eq. (65) and the linear relationship among the ξ moments $\langle\xi^{\parallel;n}_{2;\phi}\rangle|_\mu$ and the Gegenbauer moments $a^n_{2;\phi}(\mu)$, one can derive the ξ moments at any scale μ.

B. Determination of ϕ-meson leading-twist LCDA

Two crucial parameters need to be established when determining the moments of LCDA within the framework of BFTSR. Within an appropriate Borel window, the zeroth-order Gegenbauer moment is normalized to determine the continuum threshold, namely, $s_\phi=2.1\ \text{GeV}^2$. When determining the Borel parameters, it is necessary for the contributions from the continuum states and the six-dimensional condensates to be sufficiently small. Numerically, we have found that reasonable Borel windows can be achieved by constraining the contributions from the continuous states for the first five moments as 20%, 25%, 30%, 35%, and 40%, respectively; and the contributions from the six-dimensional condensation for all moments are no more than 5%.

As a conservative prediction, we stipulate that the variations of $\langle\xi^{\parallel;n}_{2;\phi}\rangle|_\mu$ within the Borel window should be less than 10%. Figure 2 shows how the first five nonzero moments of ϕ-meson longitudinal leading-twist LCDA at $\mu=\sqrt{M^2}$ GeV change with the Borel parameter M^2. The shaded bands represent the corresponding Borel windows, each falling within the region of $[1.0, 5.0]\ \text{GeV}^2$. At the scale $\mu_0=1$ GeV, we have

$$\langle\xi^{\parallel;2}_{2;\phi}\rangle|_{\mu_0}=0.199\pm 0.010, \tag{67}$$

$$\langle\xi^{\parallel;2}_{4;\phi}\rangle|_{\mu_0}=0.086\pm 0.006, \tag{68}$$

$$\langle\xi^{\parallel;2}_{6;\phi}\rangle|_{\mu_0}=0.049\pm 0.004, \tag{69}$$

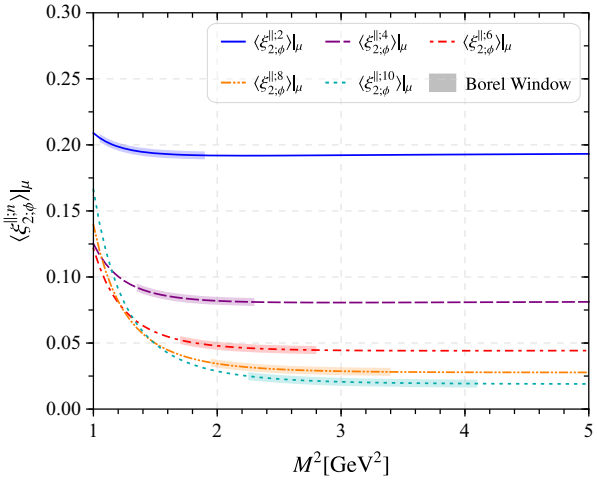

FIG. 2. Moments of the leading-twist LCDA $\langle\xi^{\parallel;n}_{2;\phi}\rangle|_{\mu=\sqrt{M^2}}$ up to $n=(2,4,6,8,10)$-order level versus the Borel parameter M^2. The shaded bands stand for the corresponding Borel windows.

$$\langle \xi^{\|;2}_{8;\phi}\rangle|_{\mu_0} = 0.032 \pm 0.003, \tag{70}$$

$$\langle \xi^{\|;2}_{10;\phi}\rangle|_{\mu_0} = 0.022 \pm 0.003. \tag{71}$$

Using the relationships (13)–(15), … among $\langle \xi^{\|;n}_{2;\phi}\rangle|_\mu$ and $a^n_{2;\phi}(\mu)$, the values of $a^n_{2;\phi}(\mu)$ at the scale $\mu_0 = 1$ GeV can be obtained accordingly. By applying the evolution equation, the values of $\langle \xi^{\|;n}_{2;\phi}\rangle|_\mu$ and $a^n_{2;\phi}(\mu)$ can be obtained at any scale. Using those values together with the constraints listed in previous section, we are ready to fix the ϕ-meson longitudinal leading-twist LCDA at any scales.

We then present the ϕ-meson leading-twist LCDA in Fig. 3. As a comparison, we have displayed the results derived from the QCD SR [41], DSE [43], BSWF [44], AM [45], and lattice QCD [46] approaches in Fig. 3. For easy comparison, all the curves are for $\mu = 2$ GeV. When $\mu = 2$ GeV, the corresponding input parameters for our present models I and II are shown in Table I. For example, when $\mu = 2$ GeV, the corresponding input parameters for our present models I and II are $A^{\|(\mathrm{I})}_{2;\phi} = 11.508\ \mathrm{GeV}^{-1}$, $\beta^{(\mathrm{I})}_{2;\phi} = 1.212$ GeV, $b^2_{2;\phi} = 0.061$, $b^4_{2;\phi} = 0.020$, and $A^{\|(\mathrm{II})}_{2;\phi} = 2.515\ \mathrm{GeV}^{-1}$, $\alpha_{2;\phi} = -0.940$, $B^2_{2;\phi} = -0.149$, $\beta^{(\mathrm{II})}_{2;\phi} = 1.207$ GeV, respectively. For convenience, Table I displays the model parameters under three typical scales, e.g., $\mu = 1$, 1.5, and 2 GeV, respectively. The usual asymptotic behavior has also been presented in Fig. 3. Previous QCD SR calculation prefers a double humped behavior [41]. In previous QCD sum rule analysis [41], the leading-twist LCDA of the ϕ meson was fixed by its analogy with the K^* meson, in which the light quark q was simply replaced by the strange quark s as an approximation. Using this approximation, Ref. [41] yielded a LCDA with a double-peak behavior; it had limitations in terms of accuracy. At present, we adopt a more rigorous treatment and take into account the s-quark mass effects throughout the calculations. Figure 3 shows that our present model I and model II are close in shape and both prefer the asymptotic form, but with different end point behaviors; since model II shows better end point behavior and is more precise, we adopt model II to do the calculation. Generally, the heavy-to-light TFFs can be dealt with by using the k_T factorization approach [86,87], according to previous experiences on the $B \to \pi$ or $B \to \rho$ TFFs [29,73]; by using this way to construct the light meson's LCDA, the end point singularity for the heavy-to-light meson transitions can also be greatly improved. Numerically, we have found that the $D_s^+ \to \phi$ TFFs and hence the related physical observables are almost the same for those two models. Such single-peak behavior is also consistent with the predictions of the lattice QCD, DSE, BSWF, AM approaches. Thus, in the following discussions, we will adopt model II for our discussion.

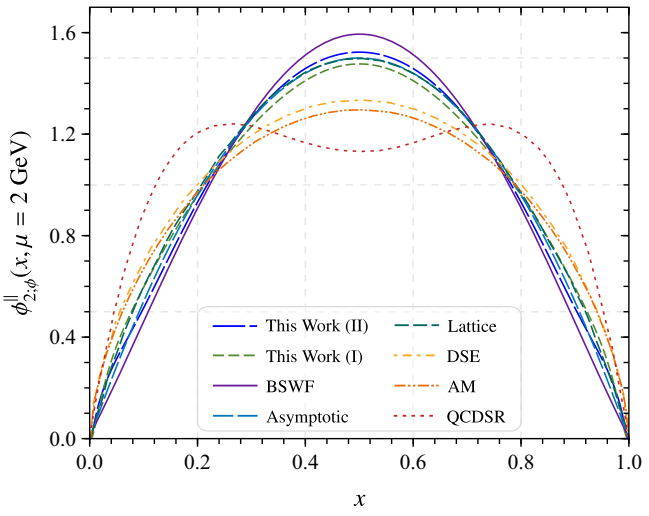

FIG. 3. Model I and II ϕ-meson longitudinal leading-twist LCDA $\phi^{\|}_{2;\phi}(x,\mu)$ at the scale $\mu = 2$ GeV. As a comparison, the results derived from the QCD SR [41], DSE [43], BSWF [44], AM [45], lattice QCD [46] approaches have been presented. The usual asymptotic behavior [68] for $\mu \to \infty$ is also presented.

As mentioned above, the typical scale for the $D_s^+ \to \phi$ TFFs is $\mu_k \approx 1.5$ GeV. For later convenience, we give the fitting parameters for $\phi^{\|}_{2;\phi}(x,\mu)$ at the scale μ_k in Table I, which gives $A^{\|(\mathrm{II})}_{2;\phi} = 5.808\ \mathrm{GeV}^{-1}$, $\alpha_{2;\phi} = -0.650$, $B^2_{2;\phi} = -0.110$, and $\beta^{(\mathrm{II})}_{2;\phi} = 0.989$ GeV, etc. Here we have implicitly set the s-quark constituent quark mass $m_s = 370$ MeV, which is given under the invariant meson mass scheme [88,89]. Under the spin-averaged meson mass scheme, Refs. [90,91] suggest that $m_s = 450$ MeV. If using this value, we observe that the input parameters will be changed accordingly, which, however, slightly changes the shape of $\phi^{\|}_{2;\phi}(x,\mu)$ and negligibly affects the magnitude of the $D_s^+ \to \phi$ TFFs. So we will adopt $m_s = 370$ MeV to do our calculations, which also results in a higher goodness of fit up to 99.6%. Practically, the probability magnitude $P_{\chi^2}(P_{\chi^2} \in [0,1])$ is employed to

TABLE I. Model I and II LCHO parameters for ϕ-meson longitudinal twist-2 LCDA with the factorization scale $\mu = (1.0, 1.5, 2.0)$ GeV for $m_s = 370$ MeV, respectively.

μ (GeV)	$A^{\|(\mathrm{I})}_{2;\phi}(\mathrm{GeV}^{-1})$	$\beta^{(\mathrm{I})}_{2;\phi}$ (GeV)	$b^2_{2;\phi}$	$b^4_{2;\phi}$
1.0	27.509	0.814	0.020	0.044
1.5	16.768	0.992	0.051	0.033
2.0	11.508	1.212	0.061	0.020
μ (GeV)	$A^{\|(\mathrm{II})}_{2;\phi}(\mathrm{GeV}^{-1})$	$\beta^{(\mathrm{II})}_{2;\phi}$ (GeV)	$\alpha_{2;\phi}$	$B^2_{2;\phi}$
1.0	10.469	0.813	−0.590	−0.110
1.5	5.808	0.989	−0.650	−0.110
2.0	2.515	1.207	−0.940	−0.149

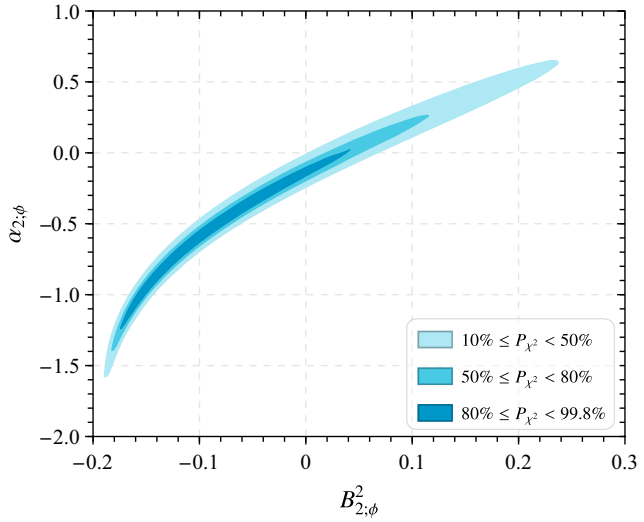

FIG. 4. The allowable regions for the combined parameters $\alpha_{2;\phi}$ and $B^2_{2;\phi}$ versus the goodness-of-fit P_{χ^2} for the case of s-quark constituent quark mass $m_s = 370$ MeV.

judge the goodness of fit [79]; when its value is closer to 1, a better fit is assumed to be achieved. To illustrate the relationship more clearly for the combined magnitudes of $\alpha_{2;\phi}$ and $B^2_{2;\phi}$ with the goodness-of-fit P_{χ^2}, we present the allowable regions for the combined parameters $\alpha_{2;\phi}$ and $B^2_{2;\phi}$ versus the goodness-of-fit P_{χ^2} in Fig. 4. In Fig. 4, the darker shaded band represents a better goodness of fit. It can be observed that, as the goodness of fit goes up, the allowable range for the combined parameters goes down.

With the resultant ϕ-meson longitudinal leading-twist LCDA, we can get the two ϕ-meson twist-3 LCDA $\phi^{\perp}_{3;\phi}(x)$ and $\psi^{\perp}_{3;\phi}(x)$ through the WW approximate relationship from Eq. (4). For convenience, we call it scenario 1 (S1). Meanwhile, there are also classical conformal expressions for the twist-3 LCDAs that correspond to the simplest self-consistent approximation suggested by Refs. [53,92].[2] In the two expressions, the second-order Gegenbauer moment $a^2_{2;\phi}$ is one of the important parameters. So for scenario 2 (S2), we will consider the newly $a^2_{2;\phi} = -0.002$ calculated within BFTSR in this paper. In order to have a clear look at the forms of twist-3 LCDA with S1 and S2, we present the curves in Fig. 5(a). We have found that both $\phi^{\perp(S1)}_{3;\phi}(x)$ and $\phi^{\perp(S2)}_{3;\phi}(x)$ exhibit single-peak behavior, and $\psi^{\perp(S2)}_{3;\phi}(x)$ is consistent with the behavior predicted in Ref. [42]. Although the curves of $\psi^{\perp(S1)}_{3;\phi}(x)$ and $\psi^{\perp(S2)}_{3;\phi}(x)$ differ significantly, their impacts on the final TFFs are consistent with each other.

[2]The detailed expressions can be seen in Eqs. (39) and (40) of Ref. [92].

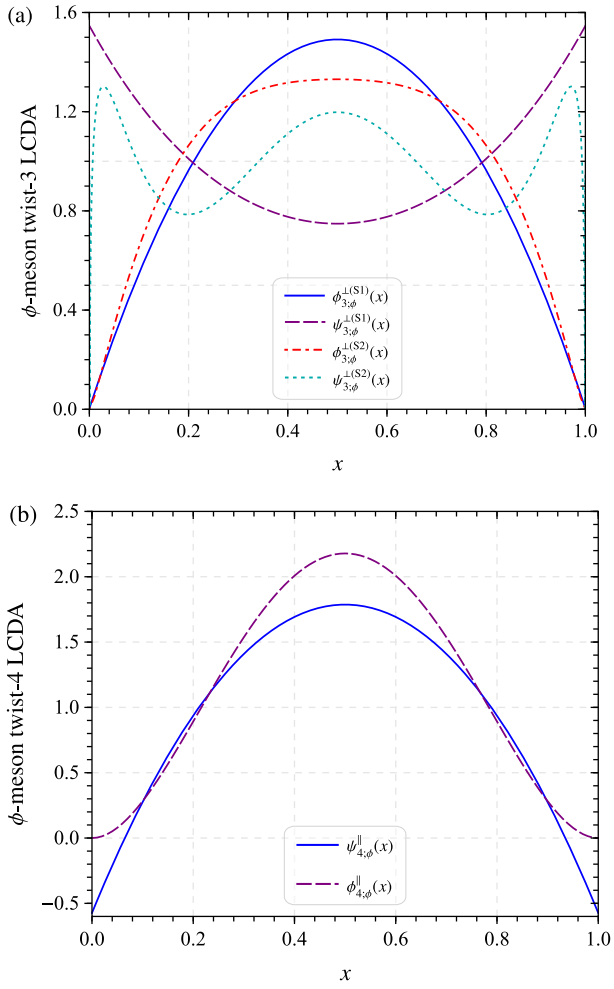

FIG. 5. (a) The behavior of ϕ-meson chiral-odd twist-3 LCDAs $\phi^{\perp}_{3;\phi}(x)$ and $\psi^{\perp}_{3;\phi}(x)$ with S1 and S2 cases. (b) Curves for ϕ-meson chiral-odd twist-4 LCDAs $\psi^{\parallel}_{4;\phi}(x)$ and $\phi^{\parallel}_{4;\phi}(x)$.

Furthermore, the detailed expressions of twist-4 LCDAs $\phi^{\parallel}_{4;\phi}(x)$, $\psi^{\parallel}_{4;\phi}(x)$ and related parameter values we used are coming from Ref. [53]. The curves are given in Fig. 5(b).

C. The $D_s^+ \to \phi$ TFFs

The continuum threshold s_0 and the Borel parameter M^2 are two important input parameters for the LCSR analysis of the $D_s^+ \to \phi$ TFFs. Usually, the continuum threshold s_0 is taken as the value that is close to the squared mass of the first excited state of D_s^+. As a conservative prediction, we set $s_0^{A_0} = s_0^{A_1} = s_0^{A_2} = s_0^V = 6.70(25)$ GeV^2 to do our discussion, whose central value is set by $D^+_{s0}(2590)$ [79]. The Borel parameter has to be chosen within the certain "window" to ensure the best stability of the physical results. The requirement for selecting stable window is as follows: the Borel parameter can not be excessively large, as higher resonance and continuum state contributions cannot be effectively suppressed; simultaneously, they should not be

TABLE II. The predictions for the $D_s^+ \to \phi$ TFFs $V(0)$, $A_0(0)$, $A_1(0)$, and $A_2(0)$ at the large recoil point $q^2 = 0$ within uncertainties coming from each input parameter for S1 and S2 cases. Meanwhile, we also listed the theoretical predictions as a comparison.

	$V(0)$	$A_0(0)$	$A_1(0)$	$A_2(0)$
This work (S1)	$0.902^{+0.040}_{-0.024}$	$0.560^{+0.025}_{-0.021}$	$0.514^{+0.024}_{-0.016}$	$0.438^{+0.093}_{-0.080}$
This work (S2)	$0.882^{+0.040}_{-0.036}$	$0.596^{+0.025}_{-0.020}$	$0.512^{+0.030}_{-0.020}$	$0.402^{+0.078}_{-0.067}$
LQCD(2001) [22]	0.85(14)	0.63(2)	0.63(2)	0.62(78)
LQCD(2011) [23]	0.903(67)	0.686(17)	0.594(22)	0.401(80)
LQCD(2013) [24]	1.059(124)	0.706(37)	0.615(24)	0.457(78)
HQEFT [12]	$0.778^{+0.057}_{-0.062}$	$-0.757^{+0.029}_{-0.039}$	$0.569^{+0.046}_{-0.049}$	$0.304^{+0.021}_{-0.017}$
HMχT [14]	1.10	1.02	0.61	0.32
CQM [15]	1.10	0.73	0.64	0.47
3PSR [10]	1.21(33)	0.53(12)	0.55(15)	0.59(11)
CLFQM(2008) [18]	0.91	0.62	0.61	0.58
CLFQM(2011) [19]	0.98	0.72	0.69	0.57
LFQM [21]	1.24	0.71	0.77	0.66
LCSR [13]	0.70(10)	0.53(9)	0.54(9)	0.57(9)
CCQM [17]	0.91	0.68	0.68	0.67
RQM [27]	0.999	0.713	0.643	0.492
SCI [28]	1.00	0.66	0.61	0.44

too small, as the truncated OPE would fail [38]. Therefore, we chose a slightly flatter section of the Borel window and the determined Borel parameters are $M_V^{2(\mathrm{S1})} = M_V^{2(\mathrm{S2})} = 2.7(1)$, $M_{A_0}^{2(\mathrm{S1})} = M_{A_0}^{2(\mathrm{S2})} = 2.5(2)$, $M_{A_1}^{2(\mathrm{S1})} = 2.0(2)$, $M_{A_1}^{2(\mathrm{S2})} = 2.2(2)$, $M_{A_2}^{2(\mathrm{S1})} = 2.15(1)$, and $M_{A_2}^{2(\mathrm{S2})} = 2.2(1)$ GeV^2, respectively. Using those parameters and the LCSRs (57)–(60), we calculate the $D_s^+ \to \phi$ TFFs and give their values at the large recoil point, i.e., $q^2 = 0$ GeV^2 in Table II, in which the results given by several groups have also been presented. The error of the TFFs end point value for S1 and S2 is between 2% and 9%. The predicted TFFs $V(0)$, $A_0(0)$, $A_1(0)$, and $A_2(0)$ show variations across different theoretical groups. Our predictions indicate a high level of consistency between the TFFs $V(0)$ and the results from LQCD(2011), whereas $A_1(0)$ and $A_0(0)$ exhibit smaller values compared to those obtained in LQCD(2011), and $A_2(0)$ is large.

Then, two ratios of the $D_s \to \phi$ TFFs are usually studied, which are defined as

$$\gamma_V = \frac{V(0)}{A_1(0)}, \qquad \gamma_2 = \frac{A_2(0)}{A_1(0)}. \tag{72}$$

Our predicted values of γ_V and γ_2 are given in Table III. Additionally, we have included results from other theoretical groups for comparison, including LQCD [22–24], LCSR [13], HQEFT [12], HMχT [14], CQM [15], 3PSR [10], CLFQM [18,19], LFQM [21], CCQM [17], RQM [27], and SCI [28]. We have also included results from different experimental collaboration groups: PDG [79], BESIII(2023) [9], *BABAR* [6], and FOCUS [5]. Table III also shows that our numerical results of the two ratios fall within the error range of LQCD(2013), BESIII(2023), and PDG.

TABLE III. Predictions for the ratio γ_V and γ_2 of $D_s^+ \to \phi$ transition within uncertainties for S1 and S2 cases. Meanwhile, theoretical and experimental results are also listed here as a comparison.

	γ_V	γ_2
This work (S1)	$1.755^{+0.008}_{-0.005}$	$0.852^{+0.135}_{-0.133}$
This work (S2)	$1.723^{+0.023}_{-0.021}$	$0.785^{+0.100}_{-0.104}$
PDG [79]	1.80 ± 0.08	0.84 ± 0.11
BESIII(2023) [9]	$1.58 \pm 0.17 \pm 0.02$	$0.71 \pm 0.14 \pm 0.02$
BABAR [6]	$1.807 \pm 0.046 \pm 0.065$	$0.816 \pm 0.036 \pm 0.030$
FOCUS [5]	$1.549 \pm 0.250 \pm 0.148$	$0.713 \pm 0.202 \pm 0.284$
LQCD(2001) [22]	1.37(7)	0.98(8)
LQCD(2011) [23]	1.52(12)	0.68(12)
LQCD(2013) [24]	1.72(21)	0.74(12)
HQEFT [12]	$1.37^{+0.024}_{-0.021}$	$0.53^{-0.010}_{-0.006}$
HMχT [14]	1.80	0.52
CQM [15]	1.72	0.73
3PSR [10]	2.20(85)	1.07(43)
CLFQM(2008) [18]	1.49	0.95
CLFQM(2011) [19]	1.42	0.83
LFQM [21]	1.61	0.86
LCSR [13]	1.19(23)	1.06(24)
CCQM [17]	1.34(27)	0.99(20)
RQM [27]	1.56	0.77
SCI [28]	1.64	0.72

We present the $D_s^+ \to \phi$ TFFs at the large recoil region $q^2 = 0$ in Table IV, in which the contribution from the

TABLE IV. $D_s^+ \to \phi$ TFFs at the large recoil region $q^2 = 0$ for S1 and S2 cases, in which the twist-2, 3, 4 LCDA contributions are presented separately.

	$V^{(\mathrm{S1})}(q^2)$	$A_0^{(\mathrm{S1})}(q^2)$	$A_1^{(\mathrm{S1})}(q^2)$	$A_2^{(\mathrm{S1})}(q^2)$
$\Phi_{2;\phi}^{\parallel}(x)$	⋯	−0.785	⋯	2.075
$\phi_{3;\phi}^{\perp(\mathrm{S1})}(x)$	⋯	1.409	0.473	−2.049
$\psi_{3;\phi}^{\perp(\mathrm{S1})}(x)$	0.902	⋯	⋯	⋯
$\Phi_{4;\phi}^{\parallel}(x)$	⋯	−0.159	⋯	0.550
$\bar{G}_3(x)$	⋯	0.095	0.041	−0.138
Total	0.902	0.560	0.514	0.438
	$V^{(\mathrm{S2})}(q^2)$	$A_0^{(\mathrm{S2})}(q^2)$	$A_1^{(\mathrm{S2})}(q^2)$	$A_2^{(\mathrm{S2})}(q^2)$
$\Phi_{2;\phi}^{\parallel}(x)$	⋯	−0.785	⋯	2.007
$\phi_{3;\phi}^{\perp(\mathrm{S2})}(x)$	⋯	1.445	0.475	−1.986
$\psi_{3;\phi}^{\perp(\mathrm{S2})}(x)$	0.882	⋯	⋯	⋯
$\Phi_{4;\phi}^{\parallel}(x)$	⋯	−0.159	⋯	0.512
$\bar{G}_3(x)$	⋯	0.095	0.037	−0.131
Total	0.882	0.596	0.512	0.402

TABLE V. The masses of low-lying D_s resonances, coefficients $\alpha_{1,i}$, $\alpha_{2,i}$, and Δ_i of TFFs $V(q^2)$, $A_0(q^2)$, $A_1(q^2)$, and $A_2(q^2)$ for S1 and S2 cases, respectively. All the input parameters have been set to be their central values.

	$V^{(S1)}(0)$	$A_0^{(S1)}(0)$	$A_1^{(S1)}(0)$	$A_2^{(S1)}(0)$
$m_{R^*,i}$	2.1121	2.4595	2.4595	2.4595
$\alpha_{1,i}$	−11.272	−3.395	−0.605	−5.136
$\alpha_{2,i}$	301.760	111.495	53.470	166.585
Δ_i	0.064%	0.045%	0.039%	0.063%
	$V^{(S2)}(0)$	$A_0^{(S2)}(0)$	$A_1^{(S2)}(0)$	$A_2^{(S2)}(0)$
$\alpha_{1,i}$	−11.852	−5.031	−4.034	−2.562
$\alpha_{2,i}$	354.663	125.030	87.102	11.467
Δ_i	0.076%	0.045%	0.033%	0.009%

LCDAs with various twist structures are presented. Table IV shows that the contribution of $V(q^2)$ is entirely derived from the twist-3 LCDA, and the contribution of $A_1(q^2)$ mainly comes from the twist-3 LCDA and $\bar{G}_3(x)$, while the main contributions of $A_2(q^2)$ and $A_0(q^2)$ are from the twist-2 and twist-3 LCDAs. In comparison, the contributions of twist-4 LCDA and $\bar{G}_3(x)$ are relatively small. From this, it can be observed that the twist-3 LCDA is also quite significant.

The LCSR approach is applicable in low and intermediate q^2 regions, e.g., $q^2 \in [0, 0.54\ \mathrm{GeV}^2]$, and we need to extrapolate the TFFs to all allowable physical regions so as to derive the wanted values for the physical observables such as the decay widths and so on. In the present paper, we adopt the approach of simplified series expansion (SSE) [72,93] to do the extrapolation. One of the advantages of this parametrization is the simplicity to translate the near-threshold behavior of the form factors into a useful constraint on the expansion coefficients.

So the TFFs take the following form:

$$F_i(q^2) = \frac{1}{1 - q^2/m_{R^*,i}^2} \sum_{k=1}^{2} \alpha_{k,i} z^k(t, t_0). \tag{73}$$

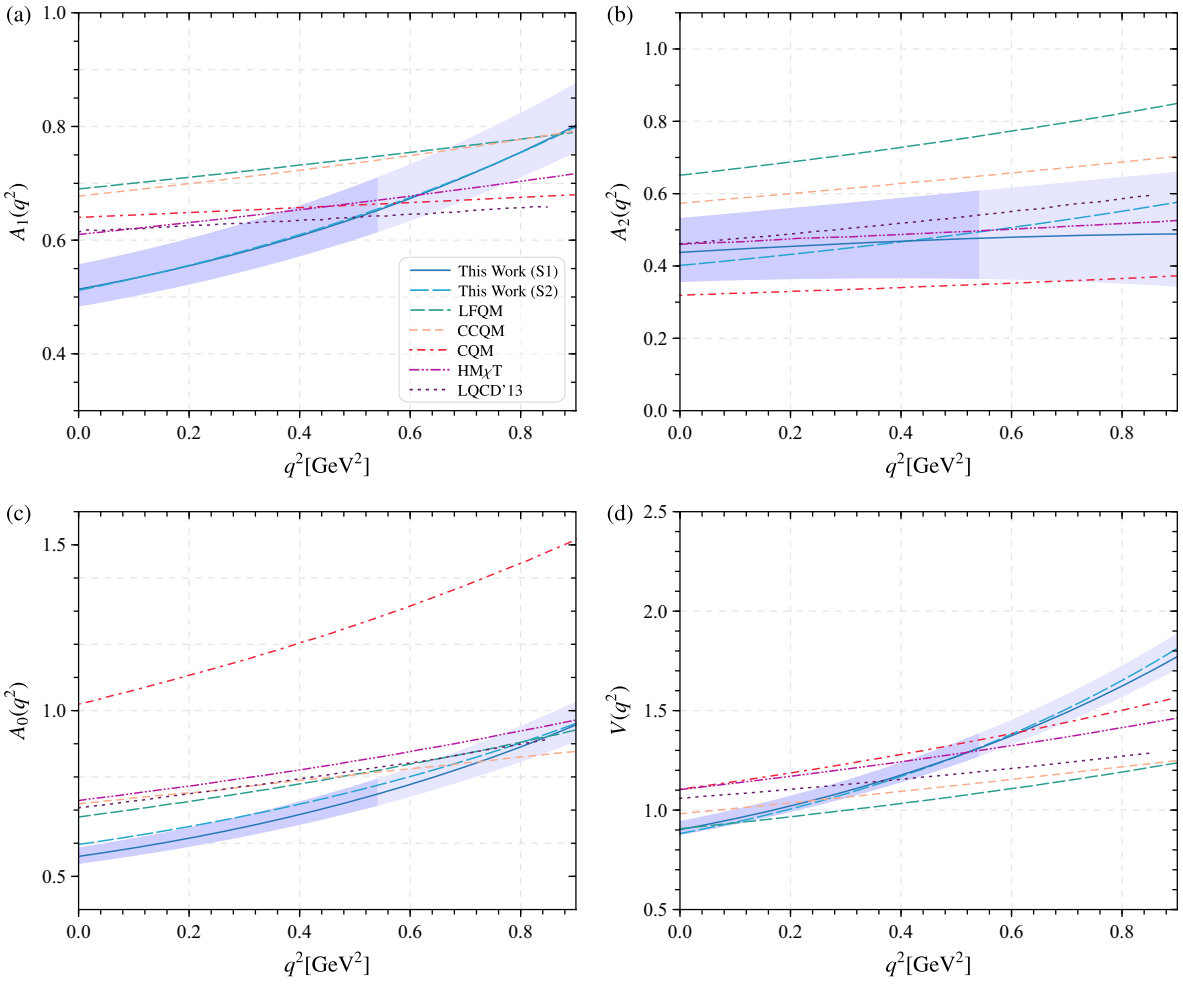

FIG. 6. The extrapolated TFFs (a) $A_1(q^2)$, (b) $A_2(q^2)$, (c) $A_0(q^2)$, and (d) $V(q^2)$ in the whole q^2 region for S1 and S2 cases, where the solid lines are central values and the shaded bands are corresponding uncertainties for S1. The thicker shaded band shows the LCSR prediction. The HMχT [14], CQM [15], CCQM [17], CLFQM(2011) [19], LQCD(2013) [24] predictions are also presented.

Here $F_i(q^2)$ with $i = (1, \ldots, 4)$ represents the four TFFs $V(q^2)$ and $A_{0,1,2}(q^2)$, respectively. The function $z(t = q^2, t_0)$, which incorporates the parameters $t_\pm$, t_0, and t, is defined as

$$z(t, t_0) = \frac{\sqrt{t_+ - t} - \sqrt{t_+ - t_0}}{\sqrt{t_+ - t} + \sqrt{t_+ - t_0}}, \tag{74}$$

where

$$t_\pm = (m_{D_s^+} \pm m_\phi)^2, \qquad t_0 = t_+(1 - \sqrt{1 - t_-/t_+}). \tag{75}$$

In this approach, the simple pole $(1 - q^2/m_{R^*,i}^2)$ is used to account for the low-lying resonances, and $m_{R^*,i}$ are D_s^+-meson resonances. The masses of the low-lying D_s^+ resonances are mainly determined by their J^P states, whose values can be found in Refs. [79,94]. The free parameters $\alpha_{1,i}$ and $\alpha_{2,i}$ are fixed to make the Δ_i as small as possible, such as $\Delta_i < 1\%$, where Δ_i is used to measure the quality of extrapolation and is defined as

$$\Delta_i = \frac{\sum_t |F_i(t) - F_i^{\rm fit}(t)|}{\sum_t |F_i(t)|} \times 100, \tag{76}$$

where $t \in [0, 1/40, \ldots, 40/40] \times 0.54\ \text{GeV}^2$. We present the masses of the low-lying D_s^+ resonances, the fitting parameters α_i for each TFF, and the quality-of-fit Δ in Table V. It shows that, under those choices of parameters, all the Δ_i values of $D_s^+ \to \phi$ TFFs are no more than 0.076%, indicating a good agreement of the extrapolated curves with the LCSRs within the same q^2 region of $q^2 \in [0, 0.54\ \text{GeV}^2]$.

Figure 6 displays the extrapolated $D_s^+ \to \phi$ TFFs across the entire q^2 region, where the results under the HMχT [14], CQM [15], CCQM [17], CLFQM(2011) [19], and LQCD(2013) [24] predictions are also presented. Here, for convenience, we only present the uncertainties for the S1 case shown in Fig. 6, while the uncertainties for the S2 case are listed in the numerical values in the following tables. The situations are same for Figs. 7 and 8. The shaded bands of our predictions are caused by the input parameters, and the results of other groups are their central predictions. Within the entire physical region, the TFFs predicted by the two distinct twist-3 LCDAs exhibit an overall consistent trend, with minor discrepancies observed at the end points. The slope of the obtained TFFs in Fig. 6 is generally larger than other theoretical groups, which is coursed by the following reasons:

(i) We have used the SSE parameterizations for extrapolation, while other theoretical groups have adopted the double-pole parameterization method. Different parameterization methods will have a certain impact on the slope. The reason why we chose SSE parameterizations is that they effectively transform the near-threshold behavior of TFFs into a constraint on the expansion coefficients.

(ii) The TFFs at large recoil region, i.e., $A_0(0)$, $A_1(0)$, and $V(0)$, which are slightly smaller than other groups, are possibly due to our selection of a flatter Borel parameter.

(iii) In this calculation, we will take the correlator with left-handed chiral current. The vector meson LCDAs have many complex structures, and it is convenient to arrange them via the parameter $\delta \simeq m_\phi/m_c \sim 0.68$. At the twist-4 accuracy, vector mesons have 15 DAs [95]. The advantage of the left-handed chiral current is that it can highlight the contributions of the δ^1- and δ^3-order DAs, while the contributions of the δ^0- and δ^2-order DAs are neglected, resulting in a different overall trend. The corresponding DAs of $\delta^{0,1,2,3}$ order are shown in Table VI. In this table, $\Phi_{3;\phi}^{\parallel}$ and $\tilde{\Phi}_{3;\phi}^{\parallel}$ represent the contributions from the three-particle part accordingly, which we have neglected in our calculations due to negligible contributions.

Using those TFFs together with the formula (44), we calculate the differential decay width $1/|V_{cs}|^2 d\Gamma(D_s^+ \to \phi \ell^+ \nu_\ell)/dq^2$, and the results are presented in Fig. 7. Throughout the entire q^2 region, the predicted decay widths based on the two distinct twist-3 LCDAs demonstrate a coherent overall trend, with the decay width predicted under the S1 cases being notably smaller at the end points. It shows that our differential decay width exhibits a significant deviation from other results in the low q^2 region. This is reasonable, since the decay width is

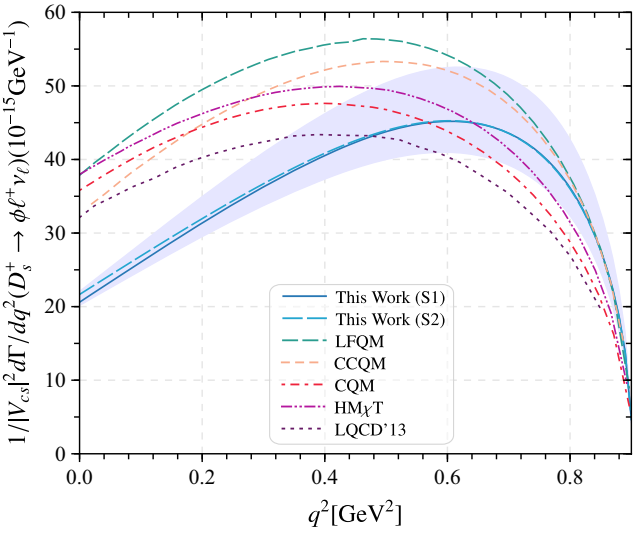

FIG. 7. The differential decay width $1/|V_{cs}|^2 d\Gamma(D_s^+ \to \phi \ell^+ \nu_\ell)/dq^2$ as a function of q^2 for S1 and S2 cases, where the solid lines are central values and the shaded bands are corresponding uncertainties for S1. The HMχT [14], CQM [15], CCQM [17], CLFQM(2011) [19], LQCD(2013) [24] predictions are also presented.

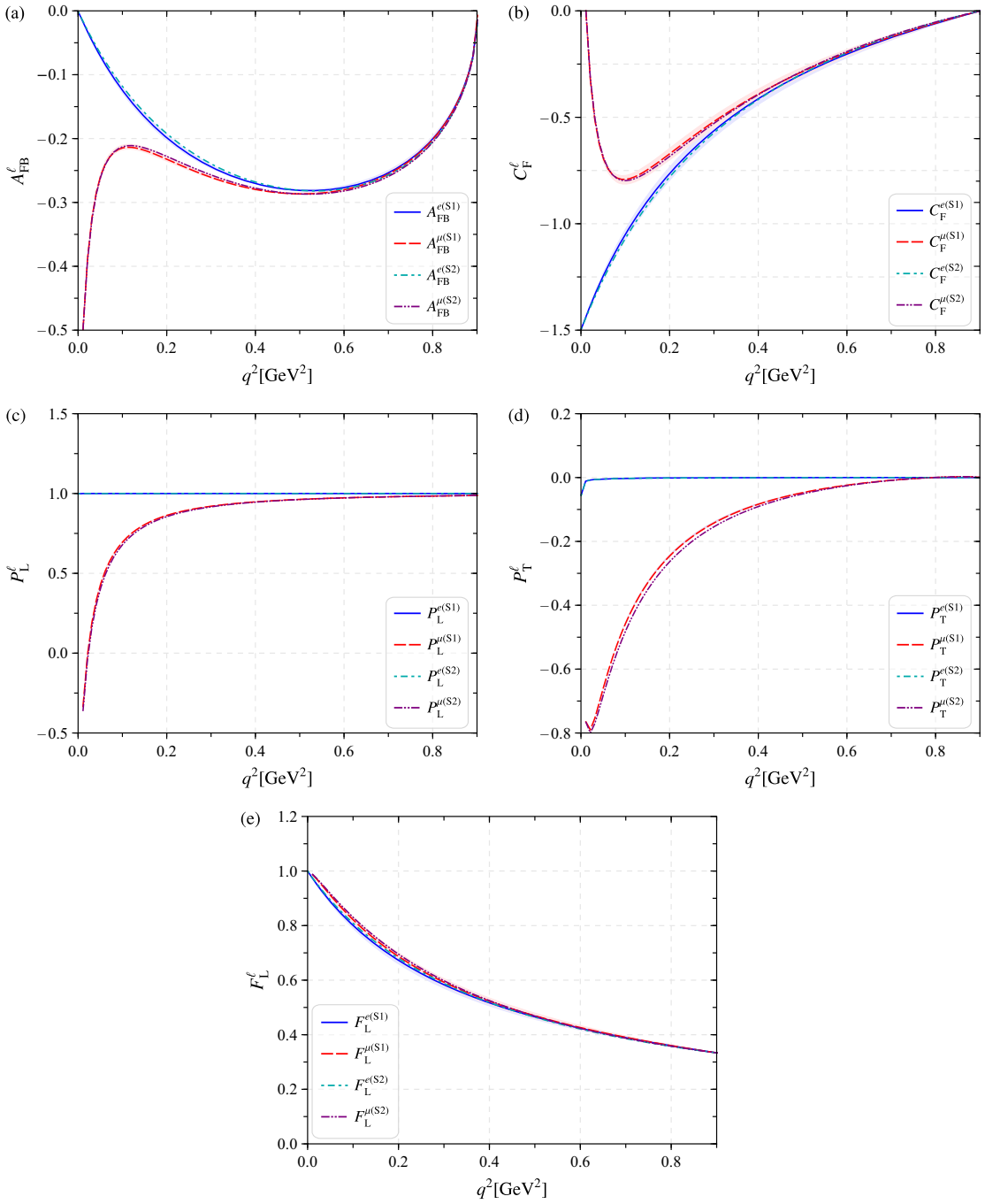

FIG. 8. The polarization and asymmetry parameters (a) $A_{\rm FB}^{\ell}$, (b) $C_{\rm F}^{\ell}$, (c) $P_{\rm L}^{\ell}$, (d) $P_{\rm T}^{\ell}$, (e) $F_{\rm L}^{\ell}$ for the semileptonic decay $D_s^+ \to \phi\ell^+\nu_\ell$ for S1 and S2 cases. The solid, dashed, and dot-dashed lines show the central values, and the shaded bands show the uncertainties for the S1 case.

dominated by the TFF $A_1(q^2)$ and we have a smaller $A_1(q^2)$ in $q^2 = 0$ as shown by Table II. Integrating them over q^2 in the entire physical q^2 region from m_ℓ^2 to $(m_{D_s^+} - m_\phi)^2$, we then obtain (in GeV)

$$\Gamma_{\rm L}^{(\rm S1)} = (16.683^{+1.989}_{-0.984}) \times 10^{-15}, \tag{77}$$

$$\Gamma_{\rm T}^{(\rm S1)} = (15.565^{+2.711}_{-1.630}) \times 10^{-15}, \tag{78}$$

$$\Gamma_{\rm total}^{(\rm S1)} = (32.248^{+4.701}_{-2.618}) \times 10^{-15}, \tag{79}$$

$$\Gamma_{\rm L}^{(\rm S2)} = (16.914^{+1.382}_{-0.532}) \times 10^{-15}, \tag{80}$$

$$\Gamma_{\rm T}^{(\rm S2)} = (15.605^{+2.133}_{-1.276}) \times 10^{-15}, \tag{81}$$

$$\Gamma_{\rm total}^{(\rm S2)} = (32.519^{+3.515}_{-1.808}) \times 10^{-15}. \tag{82}$$

TABLE VI. The ϕ-meson DAs with different twist structures up to δ^3, where $\delta \simeq m_\phi/m_c$.

Twist	δ^0	δ^1	δ^2	δ^3
2	$\phi^\perp_{2;\phi}$	$\phi^\parallel_{2;\phi}$	⋯	⋯
3	⋯	$\phi^\perp_{3;\phi}\psi^\perp_{3;\phi}\Phi^\parallel_{3;\phi}\tilde{\Phi}^\parallel_{3;\phi}$	$\phi^\parallel_{3;\phi}\psi^\parallel_{3;\phi}\Phi^\perp_{3;\phi}$	⋯
4	⋯	⋯	$\phi^\perp_{4;\phi}\psi^\perp_{4;\phi}\Psi^\perp_{4;\phi}\tilde{\Psi}^\perp_{4;\phi}$	$\phi^\parallel_{4;\phi}\psi^\parallel_{4;\phi}$

It indicates $\Gamma_L/\Gamma_T(S2) = 1.084^{+0.059}_{-0.052}$ and $\Gamma_L/\Gamma_T(S1) = 1.072^{+0.055}_{-0.050}$, which are consistent with the CLEO data $(\Gamma_L/\Gamma_T)_{exp} = 1.0 \pm 0.3 \pm 0.2$ [3] within errors.

By using the lifetime $\tau_{D_s^+} = 0.504$ ps and the CKM matrix element $V_{cs} = 0.975$ [79], we obtain the branching fractions for $D_s^+ \to \phi\ell^+\nu_\ell$ with $\ell = (e, \mu)$, which are presented in Table VII. For $\mathcal{B}(D_s^+ \to \phi e^+\nu_e)$, our result agrees well with the PDG-averaged value [79] and is consistent with other data within errors. For $\mathcal{B}(D_s^+ \to \phi e^+\nu_e)$, our prediction falls within the error range reported by the recent more precise BESIII(2023) data [9]. The branching fraction calculated using the S1 case turns out to be closer to experimental predictions, demonstrating the effectiveness of this method in addressing such issues. By using the world average of $\mathcal{B}(D_s^+ \to \phi e^+\nu_e)$, the BESIII group then issued the ratio of those two branching fractions, e.g., $\mathcal{R}_{\mu/e} = \mathcal{B}(D_s^+ \to \phi\mu^+\nu_\mu)/\mathcal{B}(D_s^+ \to \phi e^+\nu_e) = 0.94 \pm 0.08$ [9]. Our predicted value $\simeq$0.99 falls within this margin of error, aligning with the lepton universality.

D. Polarization and asymmetry parameters of $D_s^+ \to \phi\ell^+\nu_\ell$

In this subsection, we give our prediction for the polarization and asymmetry parameters of $D_s^+ \to \phi\ell^+\nu_\ell$. Those observables provide some more detailed information for the semileptonic decays of hadrons. Substituting the extrapolated TFFs $V(q^2)$ and $A_{0,1,2}(q^2)$ into Eqs. (39)–(43), we can obtain the polarization and asymmetry parameters for $D_s^+ \to \phi\ell^+\nu_\ell$. We present the polarization and asymmetry parameters A_{FB}^ℓ, C_F^ℓ, P_L^ℓ, P_T^ℓ, and F_L^ℓ versus the q^2 in Fig. 8, whose errors caused by different choices of input parameters are shown by shaded bands. In Fig. 8, we observe that the polarization and asymmetry parameters of electrons and muons exhibit distinct behavior patterns in the low q^2 region, which is mainly due to their unique physical properties and differences in interaction mechanisms. Specifically, because of its small mass, the polarization effect of electrons is not particularly significant in interactions. However, muons, due to their larger mass, experience more complex interaction mechanisms, leading to unique behaviors in their polarization and asymmetry parameters. This difference provides us with valuable clues to further explore the behavior of fundamental particles and their interactions. Figure 8 shows that all the uncertainties are small, especially for the case of longitudinal (transverse) polarization of the final charged lepton $P_{L(T)}^\ell(q^2)$, whose uncertainties are about a thousandth and are negligible.

TABLE VII. Typical experimental and theoretical predictions on the $D_s^+ \to \phi\ell^+\nu_\ell$ branching fractions and their corresponding errors (in unit 10^{-2}).

	$\mathcal{B}(D_s^+ \to \phi e^+\nu_e)$	$\mathcal{B}(D_s^+ \to \phi\mu^+\nu_\mu)$
This work (S1)	$2.347^{+0.342}_{-0.191}$	$2.330^{+0.341}_{-0.190}$
This work (S2)	$2.367^{+0.256}_{-0.132}$	$2.349^{+0.255}_{-0.132}$
BABAR [6]	$2.61 \pm 0.11 \pm 0.15$	⋯
CLEO [7]	$2.14 \pm 0.17 \pm 0.08$	⋯
BESIII(2017) [8]	$2.26 \pm 0.45 \pm 0.09$	1.94 ± 0.54
BESIII(2023) [9]	⋯	$2.25 \pm 0.09 \pm 0.07$
PDG [79]	2.39 ± 0.16	1.90 ± 0.5
CLFQM(2017) [20]	3.1 ± 0.3	2.9 ± 0.3
3PSR(2004) [10]	1.80 ± 0.50	⋯
CLFQM(2008) [18]	2.30	⋯
LCSR [13]	$2.15^{+0.27}_{-0.31}$	⋯
HQEFT [12]	$2.53^{+0.37}_{-0.40}$	$2.40^{+0.35}_{-0.40}$
CCQM [17]	3.01	2.85
CQM [15]	2.57	2.57
χUA [26]	2.12	1.94
RQM [27]	2.69	⋯
SCI [28]	2.45	2.30

After integrating the formulas, e.g., Eqs. (39)–(43), over the squared momentum transfer q^2, we get the integrated values for those observables. The main source of uncertainty in polarization and asymmetry parameters lies in the TFFs. We have decided to conduct a detailed analysis of these parameters to clearly understand the specific uncertainty caused by different TFFs. Below are the presentation results of polarization and asymmetry parameters:

$$A_{FB}^{e(S1)} = -0.191 + (^{+0.005}_{-0.009})_V + (^{+0.000}_{-0.000})_{A_0} + (^{+0.016}_{-0.012})_{A_1} + (^{+0.007}_{-0.008})_{A_2} = -0.191^{+0.000}_{-0.000},$$
$$A_{FB}^{\mu(S1)} = -0.220 + (^{+0.005}_{-0.008})_V + (^{+0.001}_{-0.001})_{A_0} + (^{+0.017}_{-0.013})_{A_1} + (^{+0.007}_{-0.008})_{A_2} = -0.220^{+0.001}_{-0.001},$$
$$C_F^{e(S1)} = -0.418 + (^{+0.006}_{-0.003})_V + (^{+0.000}_{-0.000})_{A_0} + (^{+0.011}_{-0.015})_{A_1} + (^{+0.028}_{-0.025})_{A_2} = -0.418^{+0.015}_{-0.016},$$
$$C_F^{\mu(S1)} = -0.320 + (^{+0.006}_{-0.003})_V + (^{+0.002}_{-0.001})_{A_0} + (^{+0.017}_{-0.021})_{A_1} + (^{+0.033}_{-0.026})_{A_2} = -0.320^{+0.015}_{-0.018},$$

$$
\begin{aligned}
P_{\rm L}^{e(\rm S1)} &= 0.900 + (^{+0.000}_{-0.000})_V + (^{+0.000}_{-0.000})_{A_0} + (^{+0.000}_{-0.000})_{A_1} + (^{+0.000}_{-0.000})_{A_2} = 0.900^{+0.000}_{-0.000},\\
P_{\rm L}^{\mu(\rm S1)} &= 0.784 + (^{+0.000}_{-0.000})_V + (^{+0.005}_{-0.004})_{A_0} + (^{+0.009}_{-0.007})_{A_1} + (^{+0.004}_{-0.005})_{A_2} = 0.784^{+0.001}_{-0.000},\\
P_{\rm T}^{e(\rm S1)} &= -0.001 + (^{+0.000}_{-0.000})_V + (^{+0.001}_{-0.001})_{A_0} + (^{+0.000}_{-0.000})_{A_1} + (^{+0.000}_{-0.000})_{A_2} = -0.001^{+0.000}_{-0.000},\\
P_{\rm T}^{\mu(\rm S1)} &= -0.132 + (^{+0.003}_{-0.002})_V + (^{+0.006}_{-0.007})_{A_0} + (^{+0.007}_{-0.005})_{A_1} + (^{+0.001}_{-0.000})_{A_2} = -0.132^{+0.002}_{-0.000},\\
F_{\rm L}^{e(\rm S1)} &= 0.486 + (^{+0.001}_{-0.003})_V + (^{+0.000}_{-0.000})_{A_0} + (^{+0.008}_{-0.007})_{A_1} + (^{+0.012}_{-0.015})_{A_2} = 0.486^{+0.008}_{-0.007},\\
F_{\rm L}^{\mu(\rm S1)} &= -0.482 + (^{+0.001}_{-0.003})_V + (^{+0.001}_{-0.001})_{A_0} + (^{+0.007}_{-0.006})_{A_1} + (^{+0.011}_{-0.014})_{A_2} = 0.482^{+0.008}_{-0.007},
\end{aligned}
\tag{83}
$$

$$
\begin{aligned}
A_{\rm FB}^{e(\rm S2)} &= -0.190 + (^{+0.005}_{-0.009})_V + (^{+0.000}_{-0.000})_{A_0} + (^{+0.012}_{-0.009})_{A_1} + (^{+0.006}_{-0.007})_{A_2} = -0.190^{+0.002}_{-0.003},\\
A_{\rm FB}^{\mu(\rm S2)} &= -0.220 + (^{+0.005}_{-0.009})_V + (^{+0.001}_{-0.001})_{A_0} + (^{+0.013}_{-0.009})_{A_1} + (^{+0.006}_{-0.007})_{A_2} = -0.220^{+0.002}_{-0.002},\\
C_{\rm F}^{e(\rm S2)} &= -0.421 + (^{+0.006}_{-0.003})_V + (^{+0.000}_{-0.000})_{A_0} + (^{+0.011}_{-0.015})_{A_1} + (^{+0.028}_{-0.025})_{A_2} = -0.421^{+0.016}_{-0.019},\\
C_{\rm F}^{\mu(\rm S2)} &= -0.320 + (^{+0.006}_{-0.003})_V + (^{+0.002}_{-0.001})_{A_0} + (^{+0.012}_{-0.015})_{A_1} + (^{+0.026}_{-0.024})_{A_2} = -0.320^{+0.015}_{-0.018},\\
P_{\rm L}^{e(\rm S2)} &= 0.900 + (^{+0.000}_{-0.000})_V + (^{+0.000}_{-0.000})_{A_0} + (^{+0.000}_{-0.000})_{A_1} + (^{+0.000}_{-0.000})_{A_2} = 0.900^{+0.000}_{-0.000},\\
P_{\rm L}^{\mu(\rm S2)} &= 0.780 + (^{+0.000}_{-0.000})_V + (^{+0.004}_{-0.004})_{A_0}, + (^{+0.007}_{-0.005})_{A_1} + (^{+0.004}_{-0.005})_{A_2} = 0.780^{+0.002}_{-0.001}\\
P_{\rm T}^{e(\rm S2)} &= -0.001 + (^{+0.000}_{-0.000})_V + (^{+0.001}_{-0.001})_{A_0} + (^{+0.000}_{-0.000})_{A_1} + (^{+0.000}_{-0.000})_{A_2} = -0.001^{+0.000}_{-0.000},\\
P_{\rm T}^{\mu(\rm S2)} &= -0.139 + (^{+0.003}_{-0.002})_V + (^{+0.005}_{-0.007})_{A_0} + (^{+0.006}_{-0.004})_{A_1} + (^{+0.000}_{-0.000})_{A_2} = -0.139^{+0.001}_{-0.000},\\
F_{\rm L}^{e(\rm S2)} &= 0.487 + (^{+0.001}_{-0.003})_V + (^{+0.000}_{-0.000})_{A_0} + (^{+0.007}_{-0.005})_{A_1} + (^{+0.011}_{-0.012})_{A_2} = 0.487^{+0.008}_{-0.007},\\
F_{\rm L}^{\mu(\rm S2)} &= -0.483 + (^{+0.001}_{-0.003})_V + (^{+0.006}_{-0.004})_{A_0} + (^{+0.006}_{-0.004})_{A_1} + (^{+0.010}_{-0.011})_{A_2} = 0.483^{+0.008}_{-0.007}.
\end{aligned}
\tag{84}
$$

After analyzing the uncertainty of polarization parameter $P_{\rm T(L)}^{\ell}(\ell = e\,\text{or}\,\mu)$, we have concluded that the error bars displayed in Fig. 8(c), and especially Fig. 8(d), shows they are exceptionally narrow due to less uncertainty stemming from the input parameters. We present their central values in Table VIII, where the results derived from the RQM [27] and the CCQM [17] approaches have also been presented. The polarization and asymmetry parameters exhibit variations across different lepton masses. Our predicted $A_{\rm FB}^{\ell}$, $C_{\rm F}^{\ell}$, and $P_{\rm T}^{\mu}$ fall within the range of RQM and CCQM predictions, while both $P_{\rm L}^{\ell}$ and $F_{\rm L}^{\ell}$ exhibit smaller values compared to the predictions from RQM and CCQM.

IV. SUMMARY

In this paper, we have calculated the TFFs for the semileptonic decay $D_s^+ \to \phi\ell^+\nu_\ell$ by using the QCD LCSR approach. Numerical results for those TFFs and two typical ratios γ_V and γ_2 at the large recoil point $q^2 = 0$ have been given in Tables II and III, respectively. In doing the calculation, we have suggested an improved LCHO model for the leading-twist LCDA of the ϕ meson, whose ξ moments $\langle \xi_{2;\phi}^{\|;n} \rangle|_\mu$ can be determined by using the QCD SR approach within the background field theory. To improve its accuracy, these moments have been calculated up to tenth-order accuracy. A comparison of various LCDA

TABLE VIII. The polarization and asymmetry parameters for the semileptonic decay $D_s^+ \to \phi\ell^+\nu_\ell$. All the input parameters are set to be their central values.

	$A_{\rm FB}^{e}$	$A_{\rm FB}^{\mu}$	$C_{\rm F}^{e}$	$C_{\rm F}^{\mu}$	$P_{\rm L}^{e}$	$P_{\rm L}^{\mu}$	$P_{\rm T}^{e}$	$P_{\rm T}^{\mu}$	$F_{\rm L}^{e}$	$F_{\rm L}^{\mu}$
This work (S1)	−0.191	−0.220	−0.418	−0.320	0.900	0.784	−0.001	−0.132	0.486	0.482
This work (S2)	−0.190	−0.220	−0.421	−0.320	0.900	0.780	−0.001	−0.139	0.487	0.483
RQM [27]	−0.21	−0.24	−0.49	−0.35	1.00	0.90	0.00	−0.15	0.54	0.54
CCQM [17]	−0.18	−0.21	−0.43	−0.34	1.00	0.91	−0.11	−0.14	0.53	0.50

models at 2 GeV has been shown in Fig. 3. Our model exhibits a single-peak behavior, closely resembling the conventional asymptotic form for the light mesons and the one suggested from the lattice QCD calculation.

In our investigation of the $D_s \to \phi$ transition, we have taken two types of chiral-odd twist-3 LCDAs as input parameters to do our analyses. We have accurately calculated various physical quantities pertinent to this process, including the relevant TFFs, the ratios between TFFs, the branching fractions, the decay widths, and the polarization and asymmetry parameters. Despite the notable differences in the graphical representations of those two twist-3 LCDAs, they yield highly consistent impacts on the final predicted physical quantities. This observation suggests that, within a certain range, the specific form of the distribution amplitude chosen to describe the dynamical characteristics of this decay process exhibits a degree of equivalence.

We have presented the differential decay width of the semileptonic decay $D_s^+ \to \phi \ell^+ \nu_\ell$ with $\ell = (e, \mu)$ in Fig. 7 and the branching fractions in Table VII. For both the electron and muon channels, our predicted branching fractions are consistent with the experimental data within errors. Additionally, we have calculated its longitudinal, transverse, and total decay widths, which are shown by Eqs. (77)–(82). They indicate that $\Gamma_L/\Gamma_T(S2) = 1.084^{+0.059}_{-0.052}$ and $\Gamma_L/\Gamma_T(S1) = 1.072^{+0.055}_{-0.050}$, which are consistent with the CLEO data [3] within errors. Using those results, we have also estimated the forward-backward asymmetries and the lepton-side convexity parameters, as well as the lepton and vector meson longitudinal and transverse polarization parameters, which have been collected in Table VIII and Fig. 8. Those values can be measured and tested in future experiments, which could be inversely adopted for testing the various ϕ-meson LCDA models.

ACKNOWLEDGMENTS

This work was supported in part by the National Natural Science Foundation of China under Grants No. 12347101, No. 12265010, No. 12265009, and No. 12175025, the Project of Guizhou Provincial Department of Science and Technology under Grant No. ZK[2021]024, the Graduate Research and Innovation Foundation of Chongqing, China under Grants No. CYB23011 and No. ydstd1912, and the Fundamental Research Funds for the Central Universities under Grant No. 2020CQJQY-Z003.

[1] K. Kodama *et al.* (Fermilab E653 Collaboration), A study of the semimuonic decays of the $D_{(s)}$, Phys. Lett. B **309**, 483 (1993).
[2] P. L. Frabetti *et al.* (E687 Collaboration), Measurement of the form-factors for the decay $D_s^+ \to \phi \ell^+ \nu_\ell$, Phys. Lett. B **328**, 187 (1994).
[3] P. Avery *et al.* (CLEO Collaboration), Measurement of the ratios of form-factors in the decay $D_s^+ \to \phi \ell^+ \nu_\ell$, Phys. Lett. B **337**, 405 (1994).
[4] E. M. Aitala *et al.* (E791 Collaboration), Measurement of the form-factor ratios for $D_s^+ \to \phi \ell^+ \nu_\ell$, Phys. Lett. B **450**, 294 (1999).
[5] J. M. Link *et al.* (FOCUS Collaboration), New measurements of the $D_{(s)}^+ \to \phi \mu^+ \nu$ form-factor ratios, Phys. Lett. B **586**, 183 (2004).
[6] B. Aubert *et al.* (*BABAR* Collaboration), Study of the decay $D_s^+ \to K^+ K^- e^+ \nu_e$, Phys. Rev. D **78**, 051101 (2008).
[7] J. Hietala, D. Cronin-Hennessy, T. Pedlar, and I. Shipsey, Exclusive D_s semileptonic branching fraction measurements, Phys. Rev. D **92**, 012009 (2015).
[8] M. Ablikim *et al.* (BESIII Collaboration), Measurements of the branching fractions for the semi-leptonic decays $D_s^+ \to \phi e^+ \nu_e$, $\phi \mu^+ \nu_\mu$, $\eta \mu^+ \nu_\mu$ and $\eta' \mu^+ \nu_\mu$, Phys. Rev. D **97**, 012006 (2018).
[9] M. Ablikim *et al.* (BESIII Collaboration), Studies of the decay $D_s^+ \to K^+ K^- \mu^+ \nu_\mu$, J. High Energy Phys. 12 (2023) 072.
[10] D. S. Du, J. W. Li, and M. Z. Yang, Form-factors and semileptonic decay of $D_s^+ \to \phi \bar{l} \nu$ from QCD sum rule, Eur. Phys. J. C **37**, 173 (2004).
[11] I. Bediaga and M. Nielsen, $D_{(s)}$ decays into ϕ and $f_0(980)$ mesons, Phys. Rev. D **68**, 036001 (2003).
[12] Y. L. Wu, M. Zhong, and Y. B. Zuo, $B_{(s)}.D_{(s)} \to \pi, K, \eta, \rho, K*, \omega, \phi$ transition form factors and decay rates with extraction of the CKM parameters $|V_{(ub)}|, |V_{(cs)}|, |V_{(cd)}|$, Int. J. Mod. Phys. A **21**, 6125 (2006).
[13] T. M. Aliev, M. Savci, and A. Ozpineci, Form factors of $D_s^+ \to \phi \ell \nu$ decay in QCD light cone sum rule, Eur. Phys. J. C **38**, 85 (2004).
[14] S. Fajfer and J. F. Kamenik, Charm meson resonances and $D \to V$ semileptonic form-factors, Phys. Rev. D **72**, 034029 (2005).
[15] D. Melikhov and B. Stech, Weak form-factors for heavy meson decays: An update, Phys. Rev. D **62**, 014006 (2000).
[16] N. R. Soni and J. N. Pandya, Decay $D_s^+ \to \phi \ell^+ \nu_\ell$ in covariant quark model, EPJ Web Conf. **202**, 06010 (2019).
[17] M. A. Ivanov, J. G. Körner, J. N. Pandya, P. Santorelli, N. R. Soni, and C. T. Tran, Exclusive semileptonic decays of D and D_s mesons in the covariant confining quark model, Front. Phys. (Beijing) **14**, 64401 (2019).
[18] W. Wang and Y. L. Shen, $D_s \to K, K^*, \phi$ form factors in the covariant light-front approach and exclusive D_s decays, Phys. Rev. D **78**, 054002 (2008).

[19] R. C. Verma, Decay constants and form factors of s-wave and p-wave mesons in the covariant light-front quark model, J. Phys. G **39**, 025005 (2012).
[20] H. Y. Cheng and X. W. Kang, Branching fractions of semileptonic D and D_s decays from the covariant light-front quark model, Eur. Phys. J. C **77**, 587 (2017).
[21] Q. Chang, X. N. Li, and L. T. Wang, Revisiting the form factors of $P \to V$ transition within the light-front quark models, Eur. Phys. J. C **79**, 422 (2019).
[22] J. Gill (UKQCD Collaboration), Semileptonic decay of a heavy light pseudoscalar to a light vector meson, Nucl. Phys. B, Proc. Suppl. **106**, 391 (2002).
[23] G. Donald, C. Davies, and J. Koponen, Axial vector form factors in $D_s \to \phi$ semileptonic decays from lattice QCD, Proc. Sci. LATTICE2011 (**2011**) 278.
[24] G. C. Donald, C. T. H. Davies, J. Koponen, and G. P. Lepage (HPQCD Collaboration), V_{cs} from $D_s \to \phi \ell \nu$ semileptonic decay and full lattice QCD, Phys. Rev. D **90**, 074506 (2014).
[25] F. Hussain, A. N. Ivanov, and N. I. Troitskaya, On the form-factors of the $D_s \to \phi \mu^+ \nu_\mu$ decay, Phys. Lett. B **369**, 351 (1996).
[26] T. Sekihara and E. Oset, Investigating the nature of light scalar mesons with semileptonic decays of D mesons, Phys. Rev. D **92**, 054038 (2015).
[27] R. N. Faustov, V. O. Galkin, and X. W. Kang, Semileptonic decays of D and D_s mesons in the relativistic quark model, Phys. Rev. D **101**, 013004 (2020).
[28] H. Y. Xing, Z. N. Xu, Z. F. Cui, C. D. Roberts, and C. Xu, Heavy + heavy and heavy + light pseudoscalar to vector semileptonic transitions, Eur. Phys. J. C **82**, 889 (2022).
[29] T. Huang and X. G. Wu, Consistent calculation of the B to pi transition form-factor in the whole physical region, Phys. Rev. D **71**, 034018 (2005).
[30] M. A. Shifman, A. I. Vainshtein, and V. I. Zakharov, QCD and resonance physics. Theoretical foundations, Nucl. Phys. **B147**, 385 (1979).
[31] M. A. Shifman, A. I. Vainshtein, and V. I. Zakharov, QCD and resonance physics: Applications, Nucl. Phys. **B147**, 448 (1979).
[32] I. I. Balitsky, V. M. Braun, and A. V. Kolesnichenko, Radiative decay $\sigma^+ \to \rho\gamma$ in quantum chromodynamics, Nucl. Phys. **B312**, 509 (1989).
[33] V. L. Chernyak and I. R. Zhitnitsky, B meson exclusive decays into baryons, Nucl. Phys. **B345**, 137 (1990).
[34] P. Ball, V. M. Braun, and H. G. Dosch, Form-factors of semileptonic D decays from QCD sum rules, Phys. Rev. D **44**, 3567 (1991).
[35] V. M. Belyaev, A. Khodjamirian, and R. Ruckl, QCD calculation of the $B \to \pi, K$ form-factors, Z. Phys. C **60**, 349 (1993).
[36] P. Ball and V. M. Braun, Use and misuse of QCD sum rules in heavy to light transitions: The decay $B \to \rho e \nu$ reexamined, Phys. Rev. D **55**, 5561 (1997).
[37] P. Ball and R. Zwicky, $B_{d,s} \to \rho, \omega, K^*, \phi$ decay form-factors from light-cone sum rules revisited, Phys. Rev. D **71**, 014029 (2005).
[38] P. Ball and R. Zwicky, SU(3) breaking of leading-twist K and K^* distribution amplitudes: A Reprise, Phys. Lett. B **633**, 289 (2006).
[39] X. G. Wu, T. Huang, and Z. Y. Fang, SU(f)(3)-symmetry breaking effects of the B → K transition form-factor in the QCD light-cone sum rules, Phys. Rev. D **77**, 074001 (2008).
[40] G. Bell, T. Feldmann, Y. M. Wang, and M. W. Y. Yip, Light-cone distribution amplitudes for heavy-quark hadrons, J. High Energy Phys. 11 (2013) 191.
[41] P. Ball, V. M. Braun, and A. Lenz, Twist-4 distribution amplitudes of the K^* and ϕ-mesons in QCD, J. High Energy Phys. 08 (2007) 090.
[42] P. Ball and G. W. Jones, Twist-3 distribution amplitudes of K* and ϕ mesons, J. High Energy Phys. 03 (2007) 069.
[43] F. Gao, L. Chang, Y. X. Liu, C. D. Roberts, and S. M. Schmidt, Parton distribution amplitudes of light vector mesons, Phys. Rev. D **90**, 014011 (2014).
[44] F. E. Serna, R. C. da Silveira, and B. El-Bennich, D^* and D_s^* distribution amplitudes from Bethe-Salpeter wave functions, Phys. Rev. D **106**, L091504 (2022).
[45] B. Almeida-Zamora, J. J. Cobos-Martínez, A. Bashir, K. Raya, J. Rodríguez-Quintero, and J. Segovia, Light-front wave functions of vector mesons in an algebraic model, Phys. Rev. D **107**, 074037 (2023).
[46] J. Hua, M.-H. Chu, P. Sun, W. Wang, J. Xu, Y.-B. Yang, J.-H. Zhang, and Q.-A. Zhang (Lattice Parton Collaboration), Distribution amplitudes of K^* and ϕ at the physical pion mass from lattice QCD, Phys. Rev. Lett. **127**, 062002 (2021).
[47] S. J. Brodsky, T. Huang, and G. P. Lepage, The hadronic wave function in quantum chromodynamics, AIP Conf. Proc. **69**, 1000 (1981).
[48] S. J. Brodsky, T. Huang, and G. P. Lepage, Hadronic wave functions and high momentum transfer interactions in quantum chromodynamics, in *Particles and Fields-2—Proceedings of the Banff Summer Institute, Banff, Alberta, 1981*, edited by A. Z. Capri and A. N. Kamal (Plenum, New York, 1983), pp. 143–199.
[49] G. P. Lepage, S. J. Brodsky, T. Huang, and P. B. Mackenzie, Hadronic wave functions in QCD, in *Particles and Fieds 2—Proceedings of the Banff Summer Institute, Banff Alberta, 1981*, edited by A. Z. Capri and A. N. Kamal (Plenum, New York, 1983), pp. 83–141.
[50] J. Govaerts, F. de Viron, D. Gusbin, and J. Weyers, Exotic mesons from QCD sum rules, Phys. Lett. **128B**, 262 (1983).
[51] T. Huang, X. N. Wang, X. d. Xiang, and S. J. Brodsky, The quark mass and spin effects in the mesonic structure, Phys. Rev. D **35**, 1013 (1987).
[52] T. Huang and Z. Huang, Quantum chromodynamics in background fields, Phys. Rev. D **39**, 1213 (1989).
[53] P. Ball and V. M. Braun, Exclusive semileptonic and rare B meson decays in QCD, Phys. Rev. D **58**, 094016 (1998).
[54] A. Ali, V. M. Braun, and H. Simma, Exclusive radiative B decays in the light cone QCD sum rule approach, Z. Phys. C **63**, 437 (1994).
[55] S. Wandzura and F. Wilczek, Sum rules for spin dependent electroproduction: Test of relativistic constituent quarks, Phys. Lett. **72B**, 195 (1977).
[56] D. D. Hu, H. B. Fu, T. Zhong, L. Zeng, W. Cheng, and X. G. Wu, $\eta^{(\prime)}$-meson twist-2 distribution amplitude within QCD sum rule approach and its application to the semi-leptonic decay $D_s^+ \to \eta^{(\prime)} \ell^+ \nu_\ell$, Eur. Phys. J. C **82**, 12 (2022).

[57] T. Zhong, X. G. Wu, Z. G. Wang, T. Huang, H. B. Fu, and H. Y. Han, Revisiting the pion leading-twist distribution amplitude within the QCD background field theory, Phys. Rev. D **90**, 016004 (2014).

[58] H. B. Fu, L. Zeng, W. Cheng, X. G. Wu, and T. Zhong, Longitudinal leading-twist distribution amplitude of the J/ψ meson within the background field theory, Phys. Rev. D **97**, 074025 (2018).

[59] H. J. Melosh, Quarks: Currents and constituents, Phys. Rev. D **9**, 1095 (1974).

[60] J. H. Yu, B. W. Xiao, and B. Q. Ma, Space-like and time-like pion-rho transition form factors in the light-cone formalism, J. Phys. G **34**, 1845 (2007).

[61] S. Kaur, C. Mondal, and H. Dahiya, Light-front holographic ρ-meson distributions in the momentum space, J. High Energy Phys. 01 (2021) 136.

[62] C. D. Lu, W. Wang, and Z. T. Wei, Heavy-to-light form factors on the light cone, Phys. Rev. D **76**, 014013 (2007).

[63] N. Dhiman and H. Dahiya, Decay constants of pseudoscalar and vector B and D mesons in the light-cone quark model, Eur. Phys. J. Plus **133**, 134 (2018).

[64] W. Qian and B. Q. Ma, Vector meson $\omega - \phi$ mixing and their form factors in light-cone quark model, Phys. Rev. D **78**, 074002 (2008).

[65] X. H. Guo and T. Huang, Hadronic wavefunctions in D and B decays, Phys. Rev. D **43**, 2931 (1991).

[66] T. Zhong, Z. H. Zhu, H. B. Fu, X. G. Wu, and T. Huang, Improved light-cone harmonic oscillator model for the pionic leading-twist distribution amplitude, Phys. Rev. D **104**, 016021 (2021).

[67] T. Zhong, X. G. Wu, and T. Huang, Heavy pseudoscalar leading-twist distribution amplitudes within QCD theory in background fields, Eur. Phys. J. C **75**, 45 (2015).

[68] G. P. Lepage and S. J. Brodsky, Exclusive processes in perturbative quantum chromodynamics, Phys. Rev. D **22**, 2157 (1980).

[69] R. H. Li, C. D. Lu, and W. Wang, Transition form factors of B decays into p-wave axial-vector mesons in the perturbative QCD approach, Phys. Rev. D **79**, 034014 (2009).

[70] J. D. Richman and P. R. Burchat, Leptonic and semileptonic decays of charm and bottom hadrons, Rev. Mod. Phys. **67**, 893 (1995).

[71] D. Bečirević, F. Jaffredo, A. Peñuelas, and O. Sumensari, New physics effects in leptonic and semileptonic decays, J. High Energy Phys. 05 (2021) 175.

[72] A. Bharucha, T. Feldmann, and M. Wick, Theoretical and phenomenological constraints on form factors for radiative and semi-leptonic B-meson decays, J. High Energy Phys. 09 (2010) 090.

[73] H. B. Fu, X. G. Wu, H. Y. Han, and Y. Ma, $B \to \rho$ transition form factors and the ρ-meson transverse leading-twist distribution amplitude, J. Phys. G **42**, 055002 (2015).

[74] H. B. Fu, X. G. Wu, and Y. Ma, $B \to K^*$ transition form factors and the semi-leptonic decay $B \to K^* \mu^+ \mu^-$, J. Phys. G **43**, 015002 (2016).

[75] W. Cheng, X. G. Wu, R. Y. Zhou, and H. B. Fu, The $B \to \rho$ helicity form factors within the QCD light-cone sum rules, Phys. Rev. D **98**, 096013 (2018).

[76] H. B. Fu, L. Zeng, R. Lü, W. Cheng, and X. G. Wu, The $D \to \rho$ semileptonic and radiative decays within the light-cone sum rules, Eur. Phys. J. C **80**, 194 (2020).

[77] T. Zhong, Y. H. Dai, and H. B. Fu, ρ-meson longitudinal leading-twist distribution amplitude revisited and the $D \to \rho$ semileptonic decay, Chin. Phys. C **48**, 063108 (2024).

[78] P. Ball and V. M. Braun, Higher twist distribution amplitudes of vector mesons in QCD: Twist-4 distributions and meson mass corrections, Nucl. Phys. **B543**, 201 (1999).

[79] R. L. Workman *et al.* (Particle Data Group), Review of particle physics, Prog. Theor. Exp. Phys. **2022**, 083C01 (2022).

[80] G. Duplancic and B. Melic, Form factors of $B, B_s \to \eta^{(\prime)}$ and $D, D_s \to \eta^{(\prime)}$ transitions from QCD light-cone sum rules, J. High Energy Phys. 11 (2015) 138.

[81] S. Narison, Mini-review on QCD spectral sum rules, Nucl. Part. Phys. Proc. **258–259**, 189 (2015).

[82] K. C. Yang, W. Y. P. Hwang, E. M. Henley, and L. S. Kisslinger, QCD sum rules and neutron proton mass difference, Phys. Rev. D **47**, 3001 (1993).

[83] W. Y. P. Hwang and K. C. Yang, QCD sum rules: $\Delta - N$ and $\Sigma^0 - \Lambda$ mass splittings, Phys. Rev. D **49**, 460 (1994).

[84] C. D. Lü, Y. M. Wang, and H. Zou, Twist-3 distribution amplitudes of scalar mesons from QCD sum rules, Phys. Rev. D **75**, 056001 (2007).

[85] Y. Zhang, T. Zhong, H. B. Fu, W. Cheng, and X. G. Wu, D_s-meson leading-twist distribution amplitude within the QCD sum rules and its application to the $B_s \to D_s$ transition form factor, Phys. Rev. D **103**, 114024 (2021).

[86] J. Botts and G. F. Sterman, Hard elastic scattering in QCD: Leading behavior, Nucl. Phys. **B325**, 62 (1989).

[87] H. N. Li and G. F. Sterman, The perturbative pion form-factor with Sudakov suppression, Nucl. Phys. **B381**, 129 (1992).

[88] W. Jaus, Relativistic constituent quark model of electroweak properties of light mesons, Phys. Rev. D **44**, 2851 (1991).

[89] H. M. Choi and C. R. Ji, Mixing angles and electromagnetic properties of ground state pseudoscalar and vector meson nonets in the light cone quark model, Phys. Rev. D **59**, 074015 (1999).

[90] Z. Dziembowski and L. Mankiewicz, Light meson distribution amplitude: A simple relativistic model, Phys. Rev. Lett. **58**, 2175 (1987).

[91] H. M. Choi and C. R. Ji, Light cone quark model predictions for radiative meson decays, Nucl. Phys. **A618**, 291 (1997).

[92] P. Ball, V. M. Braun, Y. Koike, and K. Tanaka, Higher twist distribution amplitudes of vector mesons in QCD: Formalism and twist-three distributions, Nucl. Phys. **B529**, 323 (1998).

[93] A. Bharucha, D. M. Straub, and R. Zwicky, $B \to V \ell^+ \ell^-$ in the standard model from light-cone sum rules, J. High Energy Phys. 08 (2016) 098.

[94] S. Momeni, Helicity form factors for $D_{(s)} \to A \ell \nu$ process in the light-cone QCD sum rules approach, Eur. Phys. J. C **80**, 553 (2020).

[95] H. B. Fu, X. G. Wu, H. Y. Han, Y. Ma, and H. Y. Bi, The ρ-meson longitudinal leading-twist distribution amplitude, Phys. Lett. B **738**, 228 (2014).